EPCO ENGINEERING-PHYSICS COMPANY
5515 RANDOLPH ROAD / ROCKVILLE, MARYLAND

$6.60

(5) 301 915

ENGINEERING-PHYSICS COMPANY
5515 Randolph Road
Rockville, Maryland

(6) (7) (8)

CHARACTERISTIC EMISSIONS FROM AN UNDERGROUND EXPLOSION

(9) ~~Second~~ Semi-Annual Report no. 2,

(10) By Dean Reily and Vincent Cushing

(13) NA (14) NA

(15) (16)-(19) NA (20)

Contract Number:	DA-49-146-XZ-089
Contract Expiration Date:	December 15, 1962
ARPA Order Number:	172-61
Project Code Number:	8100
Name of Contractor:	Engineering-Physics Company
Amount of Contract:	$35,057.00
Project Scientist:	Vincent J. Cushing
Phone Number:	Whitehall 2-8000
Short Title of Work:	Characteristic Emissions From An Underground Explosion

EPCO Project No. 109

(11) 3 December 1962 (12) 65p.

TABLE OF CONTENTS

FOREWORD

The work described ~~herein~~ was performed for the Defense Atomic Support Agency under the sponsorship of Advanced Research Projects Agency as a part of the VELA-UNIFORM effort and deals with research in determining the seismic wave shapes emitted from an underground nuclear explosion. Cont'd on p. 4

The authors wish to acknowledge interesting technical discussions with Harold Brode of Rand Corporation and George Duvall of Stanford Research Institute prior to the initiation of the reported work. Additionally we wish to acknowledge considerable technical assistance and critical reading of the draft afforded by W. A. Losaw and George Bowden. Edward Thomas drew the numerous figures appearing in the report and assisted with the machine computations.

We should like to acknowledge also the broad and continuing assistance provided by John Lewis and Major Bruce Carswell of the Defense Atomic Support Agency.

Respectfully submitted,

ENGINEERING-PHYSICS COMPANY

Dean M. Reily

Vincent J. Cushing

CHARACTERISTIC EMISSIONS FROM AN UNDERGROUND EXPLOSION

Second Semi-Annual Report

I. INTRODUCTION

The investigation of characteristic emissions from an underground nuclear explosion described in this report represents a portion of the total effort initially undertaken by the staff of the Engineering-Physics Company in June 1961. A technical summary of the work carried out prior to this reporting period is contained in the first semi-annual report issued January 29, 1962.

The VELA-UNIFORM program was initiated for the purpose of developing techniques and equipment for the detection, at a distance, of underground nuclear explosions. One of the more difficult problems of this task is to effectively distinguish between the seismic disturbances caused by an underground nuclear explosion and those caused by earthquakes. For the purpose of developing both equipment and techniques for detection it is important that the characteristic wave shape of the mechanical disturbance be known.

Under sponsorship of the Defense Atomic Support Agency, EPCO has been given a responsibility, in connection with the VELA-UNIFORM program, to determine the shapes of seismic waves emitted from the region close to an underground nuclear explosion. The wave shapes, given in such experimentally measured quantities as particle acceleration, velocity, and displacement and expressed in terms of the properties of the medium surrounding the explosive source are of particular interest to those having the responsibility for determining whether the seismic signals received are generated by a nuclear explosion or by an earthquake. Information on wave shape will also be of interest to those designing experiments involving underground explosions.

The nature of the mechanical waves emitted from the so called non-linear region close to the explosive source has been viewed in this report as the following: the bomb is detonated and the large thermal energy release vaporizes the bomb parts as well as some of the soil in the immediate neighborhood of the source. Because of the disparity between the properties of the gas within the cavity and the soil, disturbances caused by the explosive source reverberate within the cavity and the gases soon become uniformly distributed through-out. The exceedingly large pressures within the cavity cause the cavity walls to be pushed outward rapidly tending to form a spherical room. As the walls are forced outward a spherical shock wave advances ahead crushing the soil as it propagates radially away from the explosive source. The crushed soil can be thought of as a "spherical piston" which is continually gaining mass and absorbing mechanical energy from the gas in the cavity, all the while slowing down.

In the case where the shock front velocity decreases below the small disturbance propagation velocity of the medium a new wave will be generated and this wave will propagate radially away from the front of the spherical shock wave. This disturbance is sometimes referred to as a sonic precursor. As the precursor and the main disturbance propagate to greater distances they finally reach a free surface, namely the surface of the earth, and at this instant a rarefaction wave begins to propagate back into the soil tending to relieve the compressive stress of the direct wave while conserving energy by particle acceleration. If the resultant stress produced by the combination of the rarefaction wave, compression wave, and the lithostatic pressure is a net tensile stress in excess of that required for rupture of the soil, the earth will spall and one or more slabs of soil will be hurled upward. As these slabs fall back due to gravity they impact with the underlying earth generating a secondary mechanical disturbance having a wave shape

very different from the direct disturbance initially generated by the explosive source. As the pressure in the cavity diminishes the cavity wall may no longer be able to support the crushed soil at its exterior and the cavity will collapse setting up an additional mechanical disturbance which can also be of significant magnitude.

The total problem with which we are concerned can be divided into two not altogether separable smaller problems.

1. Generation of mechanical disturbances;
2. Propagation of the resultant disturbances.

An investigation of the generation of mechanical disturbances must take into account not only the form of the initial energy of the source and the way in which it is first converted into mechanical energy but also conversions from one form of mechanical energy to another. For example, we have the case where direct mechanical waves cause a moving spall which in turn, upon impact gives up its energy in the form of a secondary wave. The problem of propagation of mechanical disturbances is complex when considered in its entirety because of geometric considerations such as lack of symmetry, irregular surfaces, layering, and so forth. Additionally the various types of geologic material and their non-linear mechanical behavior bring in the requirements for rather complex constitutive equations. The resultant equations obtained when analyzing close-in wave propagation are non-linear and of a form which will admit of solutions only by numerical methods. A complete detailed analysis of the entire wave generation and propagation problem would involve a momumental computational task which would more than exceed the practical capacity of our largest present day electronic computers. Hence we must be satisfied with a treatment of the total problem

Cont'd from p. iii

in a piecewise fashion making realistic simplifying assumptions when necessary.

~~The contents of this report are as follows. In Section II we discuss~~ the propagation of waves very close-in to the source of the explosion where the soil is subject to very high compressive forces is discussed. Results of the analysis are given in a form similar to typical experimental data--particle velocity and displacement each plotted against time, shock front arrival time, and peak particle velocity versus radial distance from the explosive source. ~~It is in this area that we are presently in process of augmenting the analysis to take into account more detailed equations of state and more accurate equations of motion. The discussion of Section III deals with~~ the transition of the disturbance to seismic waves is treated. Results are expressed in terms of particle acceleration, velocity and displacement versus time. ~~In Section IV we consider~~ the elastic precursor which propagates ahead of the main disturbance, in the event that this main disturbance at some time propagates subsonically is considered. Some qualitative results of the analysis are presented showing the wave forms expected at a hypothetical gage station. The manner in which information obtained from the precursor can aid in the determination of equation of state and other details of the wave propagation phenomena is also discussed. ~~Section V describes~~ secondary wave generation as the result of spall impact is described. ~~Investigators of underwater explosions have long been aware of the secondary waves generated in connection with the so-called bulk cavitation phenomena and consequent water hammer at impact. Experiments show that the same phenomenon is present in underground explosions. In this section we undertake~~ a rudimentary analysis is undertaken which indicates the generation of a type of mechanical disturbance quite unlike the usual body wave disturbances issued directly from the explosive source.

II. WAVES IN CRUSHABLE MEDIA

In studying wave propagation in a crushable media we must first decide upon an equation of state. Fig. 1 illustrates the equation of state to be used. We assume as a simple first model that the medium under consideration when subjected to an external mechanical force crushes, resulting in an instantaneous change from the initial density to some final density. We further assume that this final density is independent of the applied mechanical force. Dry tuff and dry alluvium behave somewhat in this fashion and while the assumption that crushing occurs instantaneously is unrealistic on a physical basis, we will find that this assumption will mainly affect the shape of the wave's leading edge. (This assumption implies that after the material has been crushed the density gradient in all directions from a given point will be zero.) We begin by neglecting the energy equation and consider only conservation of mass and momentum, thereby neglecting energy conversion to other forms. Going back to the equation of state we note that in Fig. 1 the sloping broken line represents the jump in pressure and density across the shock front; the pressure jumps from P_o to P, and hence the density jumps from ρ_o to ρ. Upon relaxation of the mechanical force from P back down to P_o the density remains constant.

We consider the following problem: a spherical cavity in a crushable medium of infinite extent. We neglect the wave propagation phenomena in the expanding gases and other materials in the cavity. We assume that the pressure in this cavity quickly attains a state where the pressure is uniform throughout the cavity. As a force exerted by this pressure on the cavity wall forces the wall away from the center of the cavity we assume the following relationship between pressure, P, in the interior gas and the location of the cavity wall

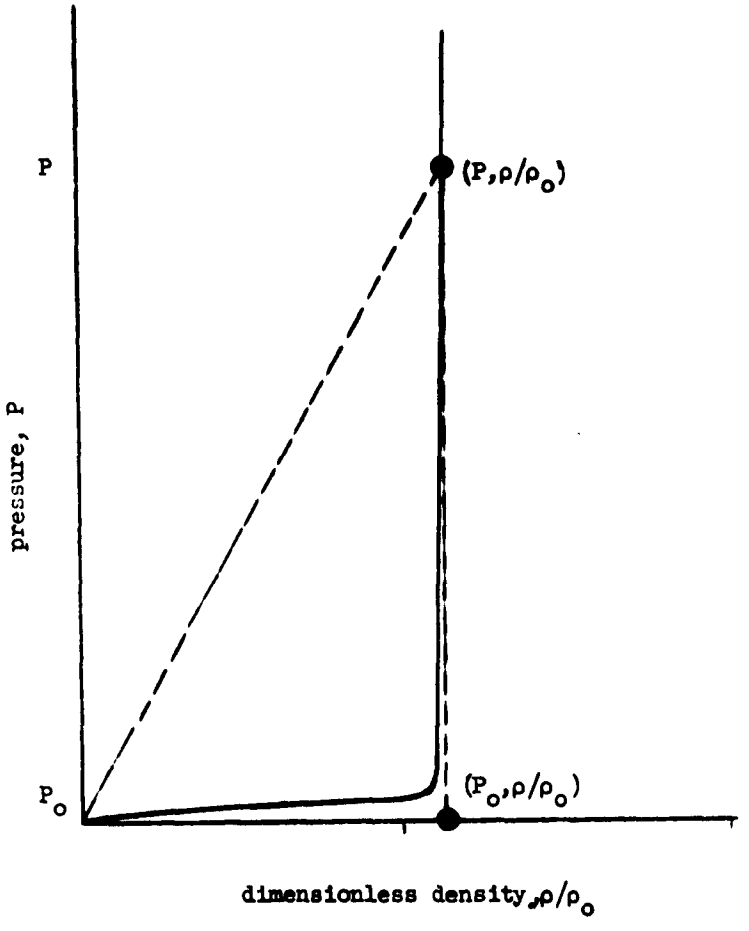

Fig. 1 --Solid curve indicates state points of shocks in the P-V plane. Sloped broken line indicates shock rise from initial pressure, P_o to peak pressure, P and dimensionless density, ρ/ρ_o. Vertical broken line indicates fall to final state at pressure, P_o and dimensionless density, ρ/ρ_o.

$$P = P_o \left(\frac{a_o}{\bar{a}_o}\right)^{3\gamma} \tag{1}$$

where P_o is the initial pressure;

a_o is the initial position of the cavity wall;

$\bar{a}_o$ is the position of the cavity wall at time, t;

γ is a constant.

Note that we also assume this wall to be impermeable in that no leakage of the gas occurs through the cavity wall. As the cavity wall is forced outward a shock wave will propagate ahead of it. This shock wave will be in the form of a spherical disturbance such that on one side the medium has experienced no mechanical motion and that at the front the material receives its first motion. Across this front we must have conservation of mass. Taking into account the equation of state previously described we have for the conservation of mass the equation

$$(R^3 - r^3)\rho_o = (R^3 - \bar{r}^3)\rho \tag{2}$$

where R is the position of the shock front measured from the cavity center;

r is the undisturbed position of a particle in the medium behind the shock front;

$\bar{r}$ is the position of the particle which was initially at r;

ρ_o is the initial density;

ρ is the final density.

Solving Eq. (2) for $\bar{r}$ we have

$$\bar{r} = [R^3(1 - \rho_o/\rho) + r^3(\rho_o/\rho)]^{1/3} \tag{3}$$

The displacement, u_r, is then given by

$$u_r = r - \bar{r} \tag{4}$$

The equation for the particle velocity, $\dot{\bar{r}}$, can be obtained directly from Eq. (3) by a differentiation with respect to t, noting that the only function which is dependent on t in Eq. (3) is R. Differentiating we obtain

$$\dot{\bar{r}} = \left(\frac{R}{\bar{r}}\right)^2 \dot{R}(1 - \rho_o/\rho) \tag{5}$$

In Eq. (1) we had written the pressure interior to the cavity in terms of the initial pressure, P_o, the initial position of the cavity wall, a_o, and the position of the cavity wall at some time, t, $\bar{a}_o$.

Using Eq. (1), we have the force exerted on a small area of the wall of the cavity at some time, t, given by

$$F_\varphi = P_o \varphi a_o^2 \left(\frac{a_o}{\bar{a}_o}\right)^{3\gamma} \tag{6}$$

where φ is a small solid angle generated from the center of the cavity and hence the impulse, I_φ, at time, t, is given by

$$I_\varphi = \int_o^t \varphi P_o a_o^{3\gamma} \bar{a}_o^{(2 - 3\gamma)} dt \tag{7}$$

The momentum, M_φ, transferred to the material which is moving as a result of the impulse given in Eq. (7) is

$$M_\varphi = \int_{\bar{a}_o}^{R} \dot{\bar{r}} dm \tag{8}$$

where dm is the mass of a segment of an elemental spherical shell.

We may express Eq. (8) in the form

$$M_\varphi = \int_{\bar{a}_o}^{R} \varphi \dot{\bar{r}} \rho \bar{r}^2 d\bar{r} \tag{9}$$

We may write the equation for momentum in a more useful form by using Eq. (3) and changing the variable of integration to obtain the expression

$$M_\varphi = \varphi \rho_o R^2 \dot{R} (1 - \rho_o/\rho) \int_{a_o}^{R} \left\{ \frac{r}{[R^3(1 - \rho_o/\rho) + r^3 \rho_o/\rho]^{1/3}} \right\}^2 dr \tag{10}$$

which is valid for any fixed time, t. Looking closely at Eq. (10), we note that this integral can be simply evaluated and we obtain the final form for the momentum given by

$$M_\varphi = \varphi \rho_o \dot{R} R^3 (1 - \rho_o/\rho) \left\{ \rho/\rho_o - (\rho/\rho_o)^{2/3} \left[(\rho/\rho_o - 1) + \left(\frac{a_o}{R}\right)^3 \right]^{1/3} \right\} \tag{11}$$

From classical mechanics the impulse must be equal to the momentum, hence we may equate Eqs. (7) and (11), obtaining

$$P_o a^{3\gamma} \int_0^t \left\{ R^3(1 - \rho_o/\rho) + a_o^3 (\rho_o/\rho) \right\}^{2/3 - \gamma} dt = \rho_o \dot{R} R^3 (1 - \rho_o/\rho) \left\{ \rho/\rho_o - (\rho/\rho_o)^{2/3} \left[(\rho/\rho_o - 1) + \left(\frac{a_o}{R}\right)^3 \right]^{1/3} \right\} \tag{12}$$

This equation is a non-linear integro-differential equation but it can be solved quite simply by numerical methods upon application of a finite difference analogue. By iterative techniques the value of t can be found while incrementing R. Using this procedure, values of R, the position of the shock front, as a function of time can be determined. From this result, using Eqs. (3) and (4), the displacement as a function of time, and from Eq. (5) the particle velocity as a function of time can be found. A subsequent differentiation of Eq. (5) will yield an ex-

pression for the particle acceleration for a particle originally at a radial distance, r.

Computer programs were written for an IBM 1620 computer to solve Eq. (12). The inputs to these computations were

1. Initial density of uncrushed soil, ρ_o.
2. Ratio of density of crushed soil to density of uncrushed soil, ρ/ρ_o.
3. Initial cavity radius, a_o.
4. The gas constant, γ.
5. The pressure in the cavity at time zero.
6. Distance from explosive source to five hypothetical gages distributed along a radial line from center.

In Fig. 2 we have illustrated the cavity wall and the five hypothetical velocity and/or displacement gages at three different times. The position of the shock front is also indicated in each case. Fig. 3 shows the displacement versus time at each of the five hypothetical displacement gages for the data described in the caption. Fig. 4 shows particle velocity versus time at each of the five hypothetical velocity gages for the same case. Fig. 5 shows the shock front arrival time for a crushable soil under the same conditions. Fig. 6 is a plot of particle velocity versus distance. This plot is again made on log-log paper so as to clearly illustrate the character of the dependency of velocity on the exponent of the distance, r. Eq. (5) shows us the relationship between Figs. 5 and 6, indicating that the particle velocity is directly dependent upon the shock velocity and position of the shock front. From further calculations it appears that the shock front velocity decrease with radial distance is affected largely by the assumed value of the constant exponent of the gas in the cavity (see Eq. (1)). Our very simple

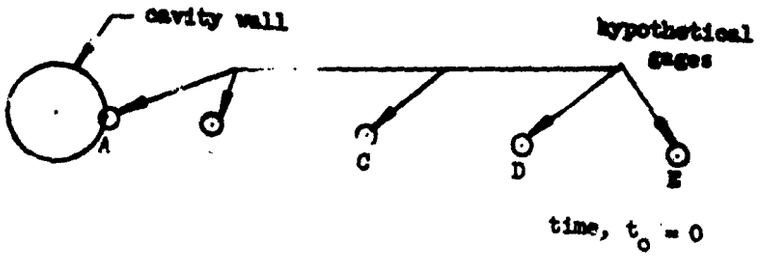

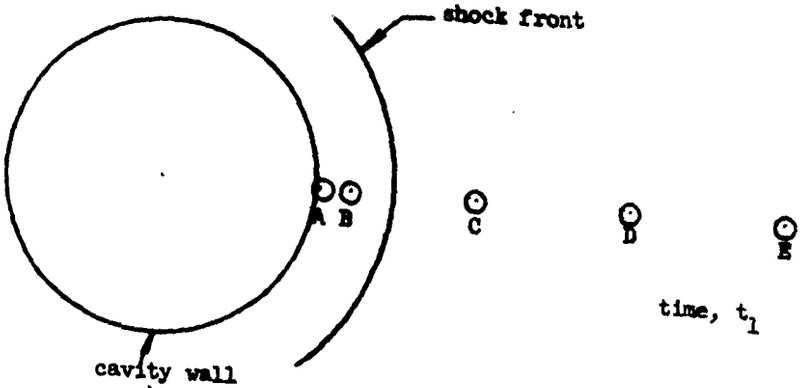

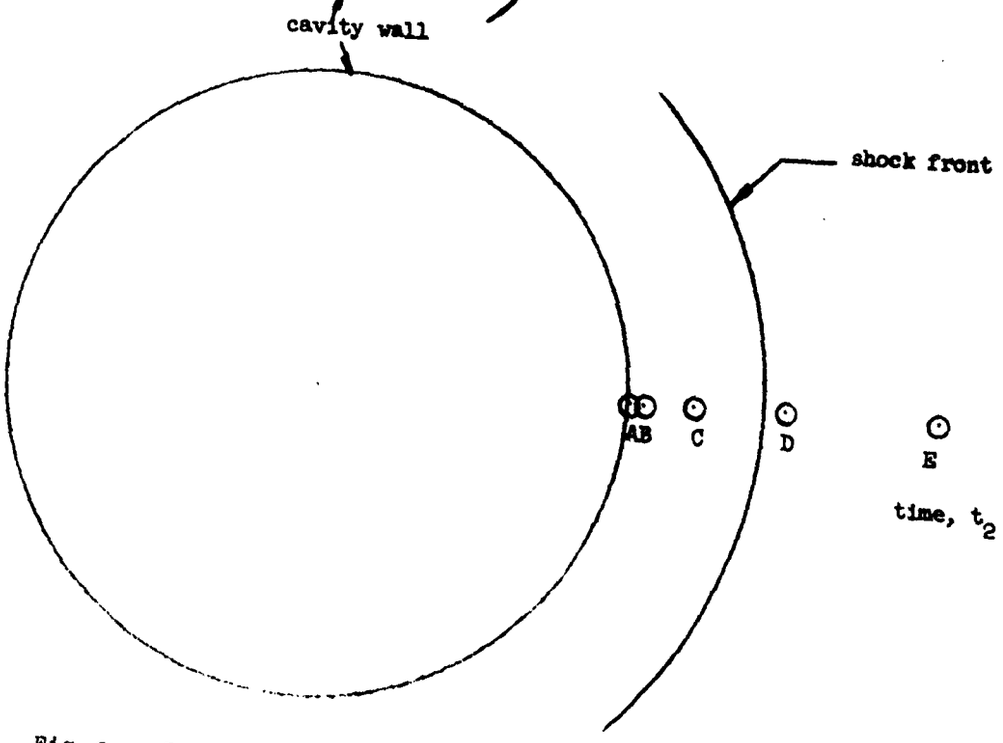

Fig. 2 --Position of cavity wall, hypothetical gages, and shock front at three different times t_o, t_1, t_2 where $t_o < t_1 < t_2$.

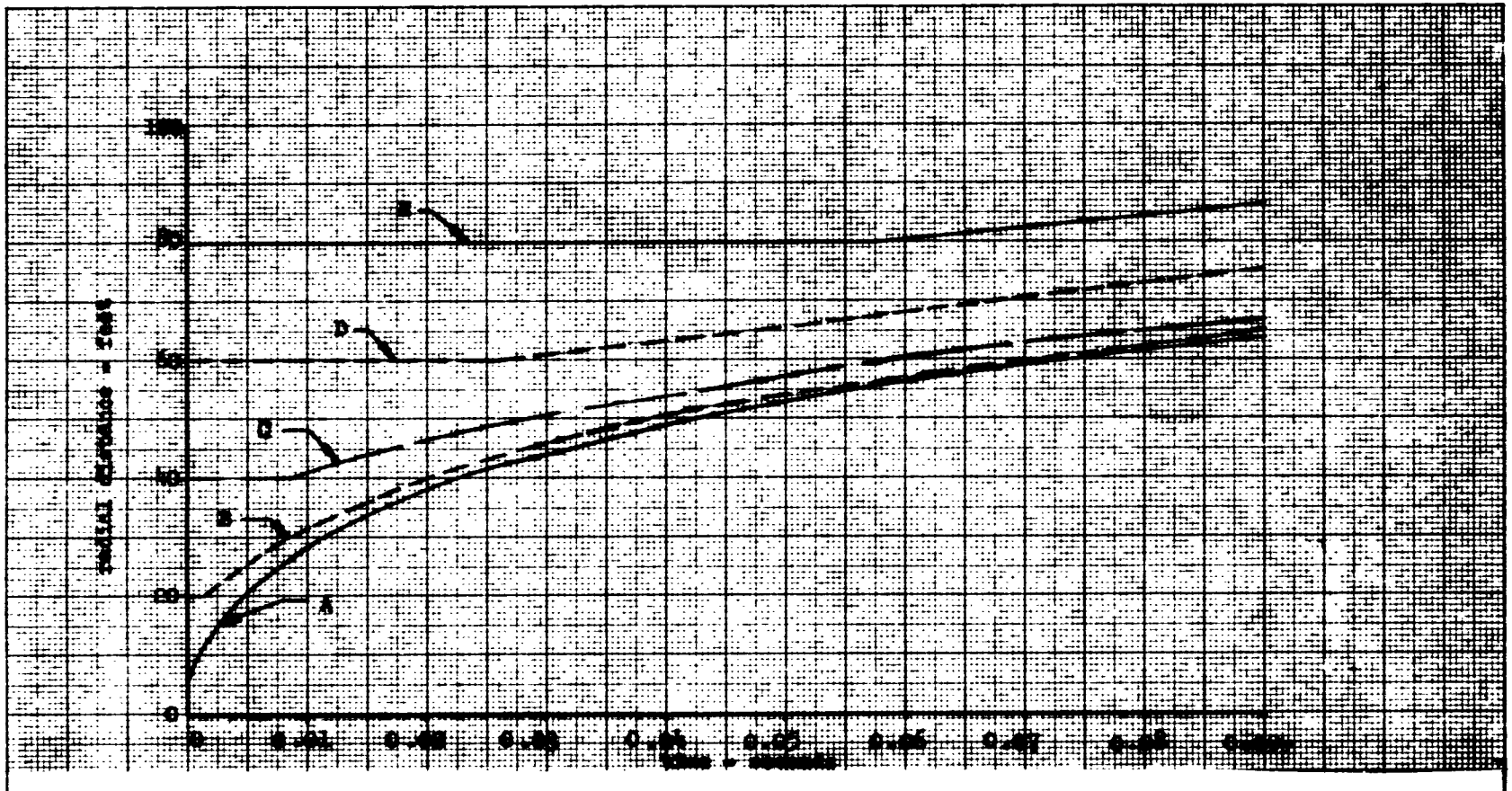

Fig. 3--Position versus time for each of five hypothetical gages where the initial configuration and soil behavior is assumed to be given by the following data $\rho_0 = 3.8$ slugs/ft.^{3}; $\rho/\rho_0 = 1.5$; $a_0 = 6$ft.; $\gamma = 1.2$; $P_0 = 2.2 \times 10^9$lb./ft.^{2}

Curves A, B, C, D and E represent the paths of the five hypothetical displacement gages.

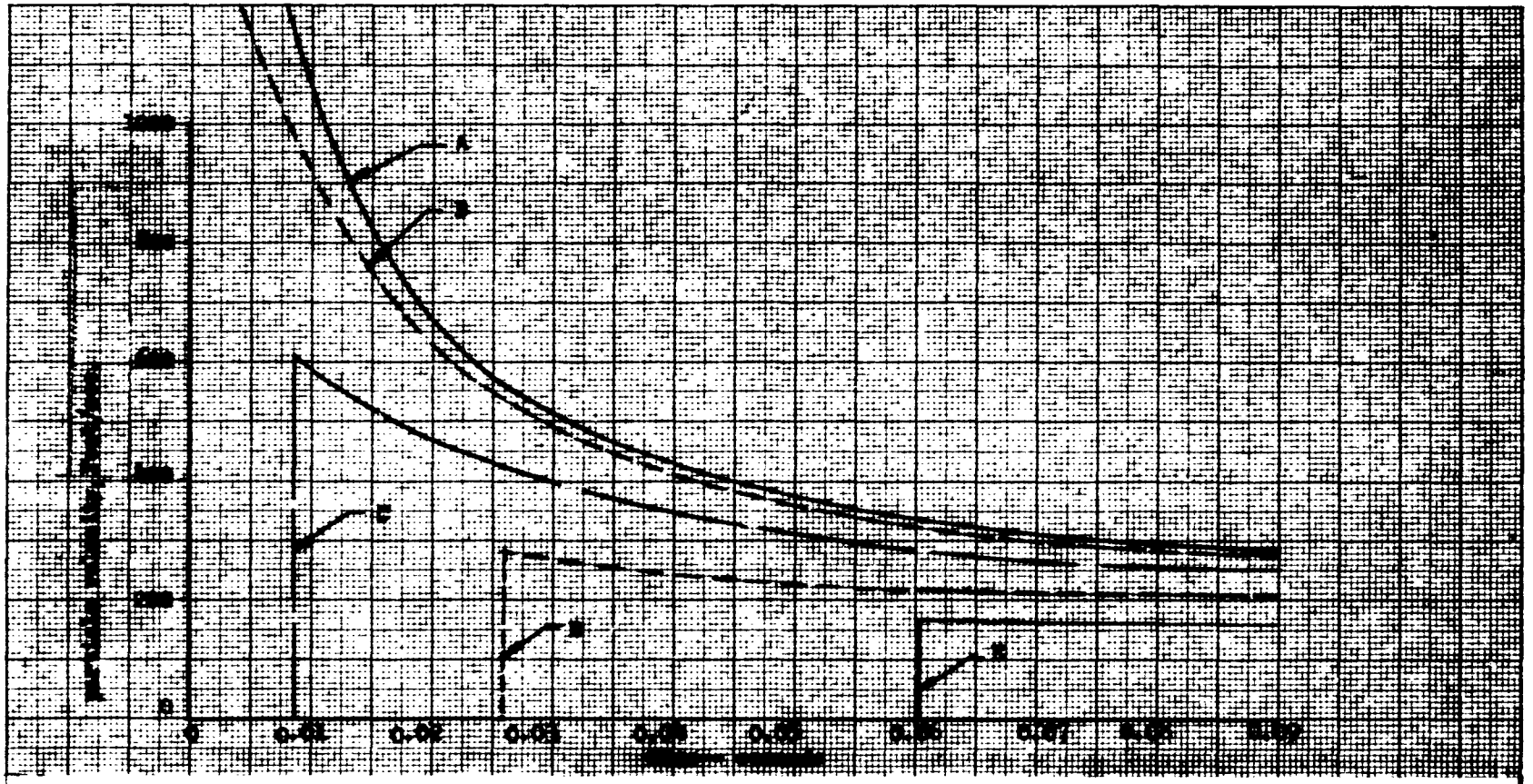

Fig. 4--Particle velocity versus time for each fo five hypothetical velocity gages for initial configuration and data given by $\rho_o = 3.8$ slugs/ft.^{3}; $\rho/\rho_o = 1.5$; $a_o = 6$ft.; $\gamma = 1.2$; $P_o = 2.2 \times 10^9$lb./ft.^{2}. Curves A, B, C, D, and E represent respectively the velocity as a function of time for each of the five hypothetical gages.

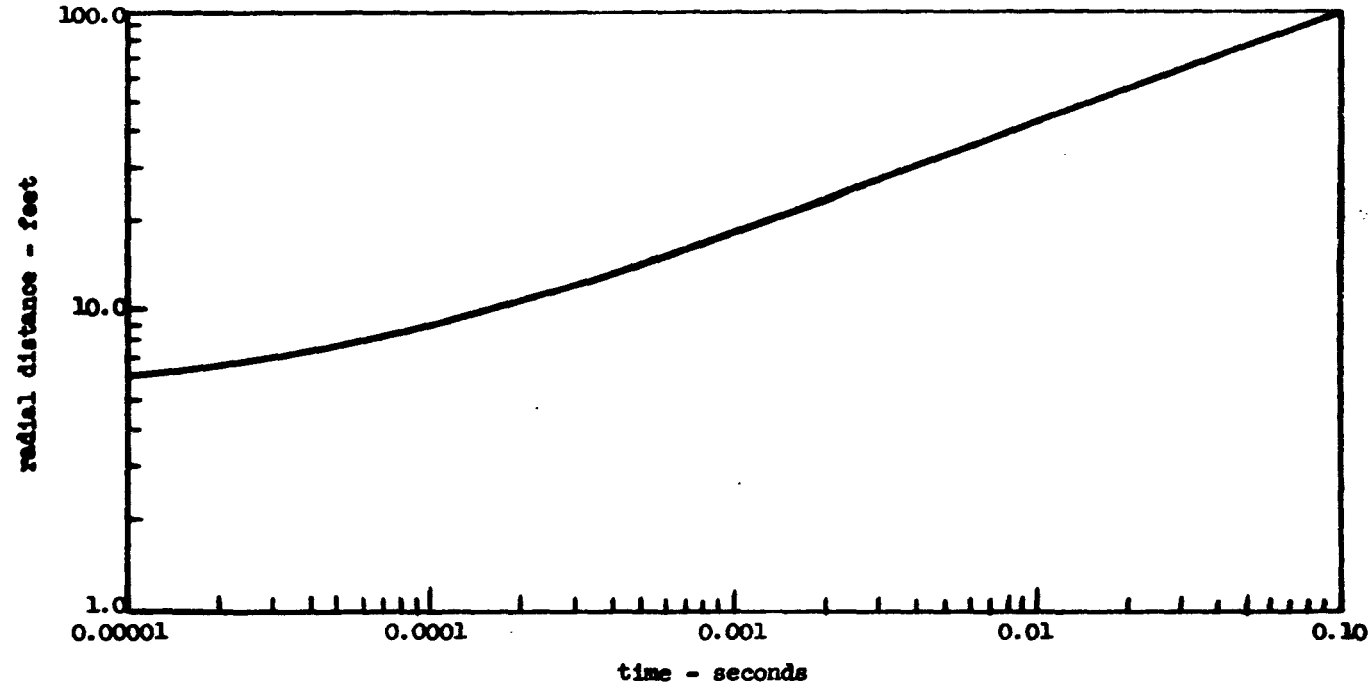

Fig. 5 --Shock front arrival time for a crushable soil under the following initial conditions ρ_o = 3.8 slugs/ft.^{3}; ρ/ρ_o = 1.5; a_o = 6ft.; γ = 1.2; P_o = 2.2 x 10^9 lb./ft.^{2}.

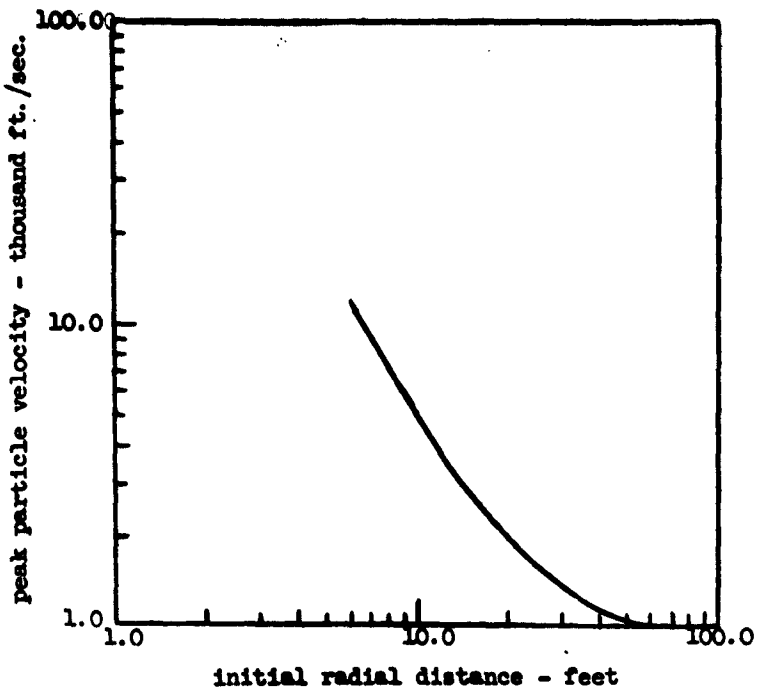

Fig.6 --Peak particle velocity measured at the hypothetical gages as a function of the initial distance of the gages from the explosive source. Initial conditions are $\rho_o = 3.8$ slugs/ft.^{3}; $\rho/\rho_o = 1.5$; $a_o = 6$ft.; $\gamma = 1.2$; $P_o = 2.2 \times 10^9$ lb./ft.^{2}.

model here assumes that the density of the crushed material is independent of the pressure level at the shock front; while for crushable materials this appears to be very nearly correct, we know from experimental evidence that in most cases the crushed density will decrease somewhat as the pressure behind the shock falls off. Such behavior would cause the plot in Fig. 6 to deviate from the straight line character shown. Figs. 7, 8, 9 and 10 are plots similar to Figs. 3, 4, 5 and 6 respectively for a different set of initial data.

The model which we have just described in no way takes into account the elastic behavior of the material, but assumes that the material is permanently crushed. In the real case, one would expect the non-porous constituent of the material to have some elastic properties under compression, and while one would expect some permanent change in the density due to crushing, there might also be a responsive change in density as a result of compressed entrapped air and the elastic properties of the other constituent materials. However, it is believed that the large changes in density will be a result of a crushing or compacting of the material, particularly in the case of porous media. As the distance from the source of the explosion increases, the material may not undergo crushing at all but simply undergo an almost elastic compression to some new density and then upon release of the applied forces be restored to its initial density. This is the behavior in the case of seismic wave propagation. In the following section we will discuss the propagation of such elastic waves.

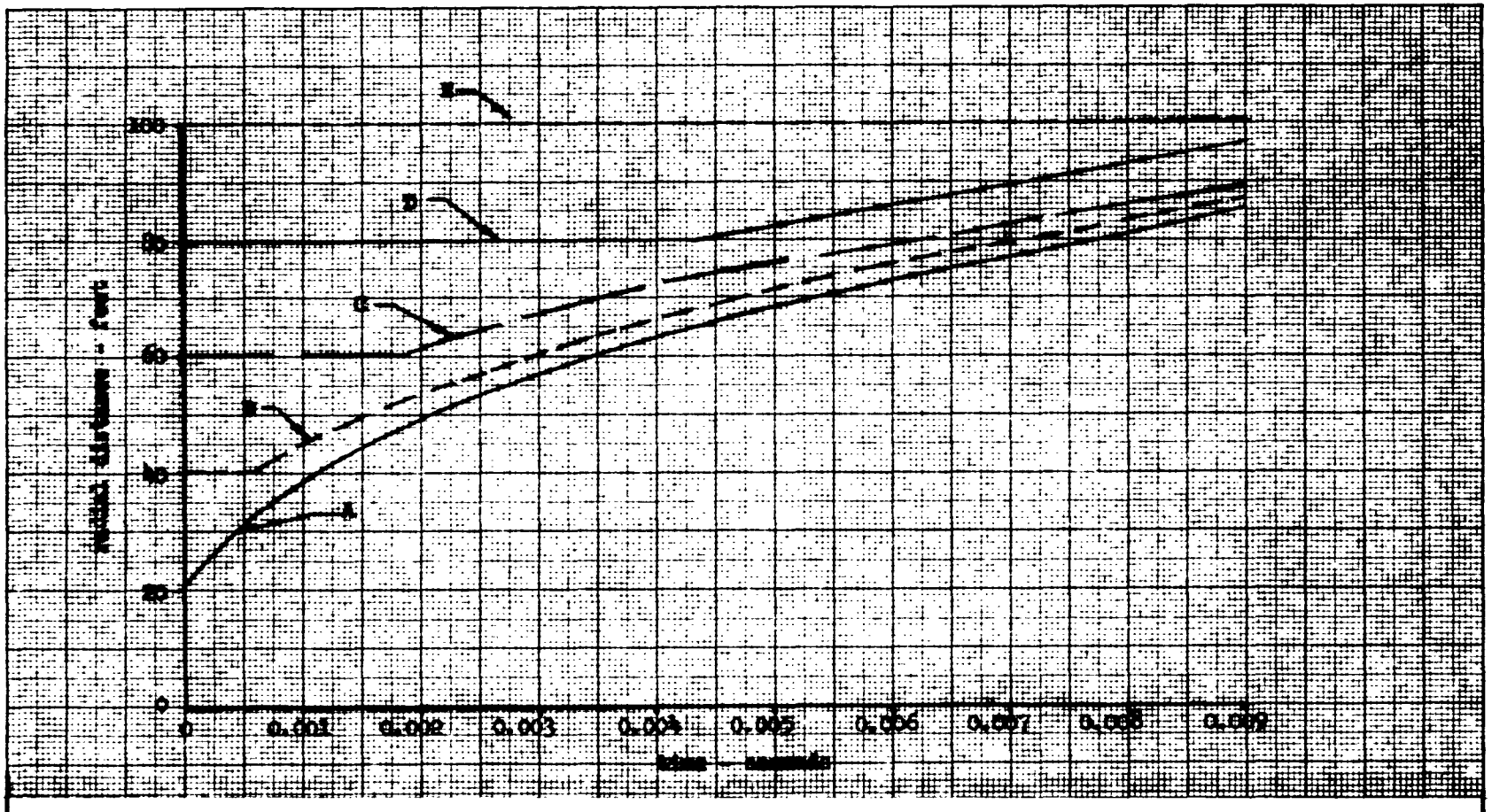

Fig. 7--Position versus time for each of five hypothetical gages where the initial configuration and soil behavior is assumed to be given by the following data. $\rho_o = 3.5$ slugs/ft.^{3}; $\rho/\rho_o = 2.0$; $a_o = 20$ft.; $\gamma = 1.2$; $P_o = 10^{10}$lb./ft.^{2}. Curves A, B, C, D and E represent the paths of the five hypothetical displacement gages.

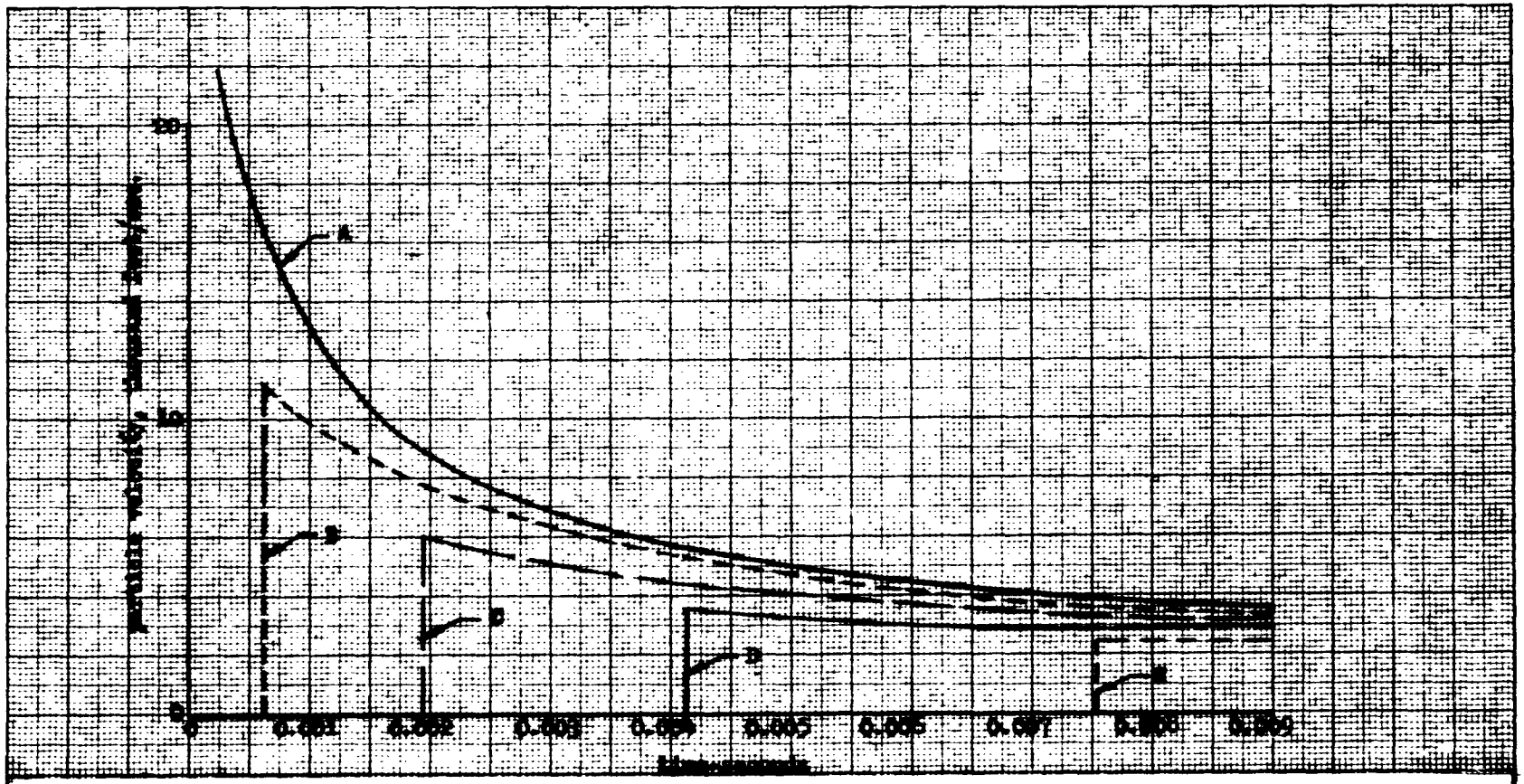

Fig. 8 --Particle velocity versus time for each of five hypothetical velocity gages for initial configuration and data given by $\rho_o = 3.5$ slugs/ft.^{3}; $\rho/\rho_o = 2.0$; $a_o = 20$ft.; $\gamma = 1.2$; $P_o = 10^{10}$lb./ft.^{2}.

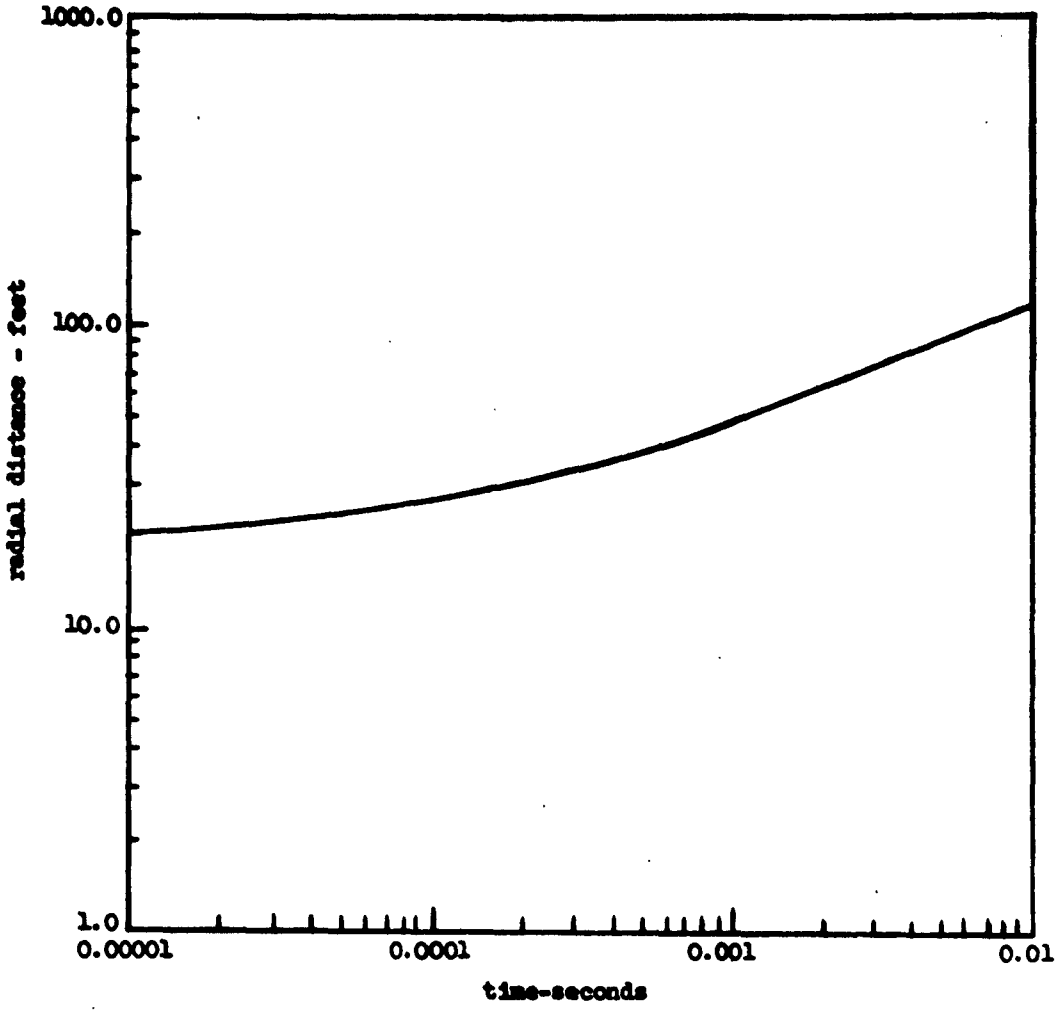

Fig. 9--Shock front arrival time for a crushable soil under the following initial conditions ρ_o = 3.5 slugs/ft.^{3}; ρ/ρ_o = 2.0; a_o = 20ft.; γ = 1.2; $P_o = 10^{10}$ lb./ft.^{2}.

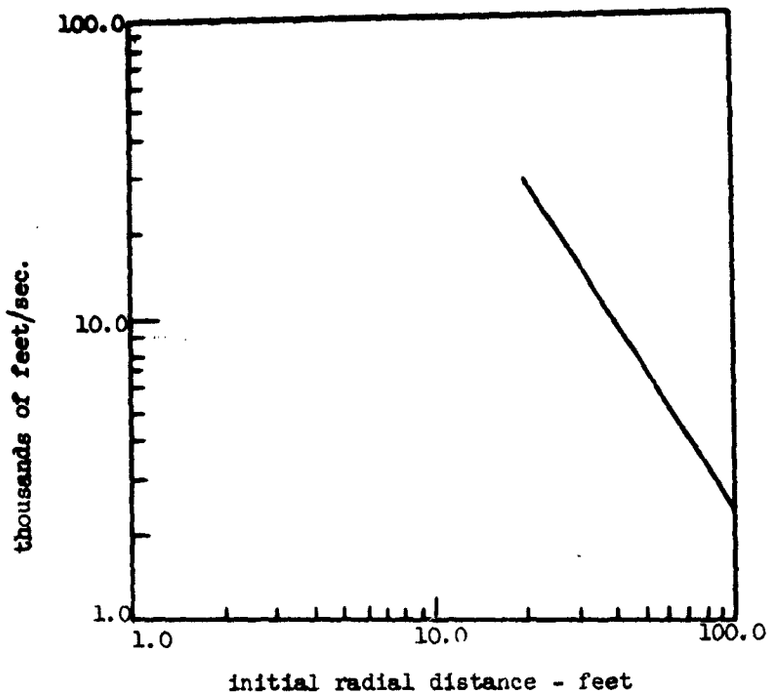

Fig. 10--Peak particle velocity measured at the hypothetical gages as a function of the initial distance of the gages from the explosive source. Initial conditions are $\rho_o = 3.5$ slugs/ft.^{3}; $\rho/\rho_o = 2.0$; $a_o = 20$ft.; $\gamma = 1.2$; $P_o = 10^{10}$lb./ft.^{2}.

III. WAVES IN MEDIA WITH ELASTIC BEHAVIOR

In the previous section we considered a wave propagating in a soil which permanently crushed or compacted to some new density different from the initial density. In this section we shall investigate the opposite extreme--the case where the density returns to its initial value after the passing of the disturbance. The true behavior would be expected to lie somewhere between these two extremes and we will make some attempt to determine the type of wave shape which we would have if the soil underwent a permanent deformation and also responded elastically. We are now concerned with relatively small deformations as compared to those considered in the equations for wave propagation in crushable material and therefore the equations describing seismic wave propagation will be linear and hence will admit of closed form solutions.

We consider a homogeneous, isotropic elastic media in which there exists a spherical boundary between the region of crushable behavior and that of seismic behavior. The soil will be assumed to extend infinitely in the radial direction away from the explosive source. We further assume that the elastic properties of the material are governed by the usual Hooke's law equations which in the case of spherical symmetry are given by

$$\sigma_r = (\lambda + 2\mu)\ (\epsilon_r + 2\epsilon_\theta) - 4\mu\epsilon_\theta \quad ; \qquad (13)$$

$$\sigma_\theta = \lambda(\epsilon_r + 2\epsilon_\theta) + 2\mu\epsilon_\theta \quad . \qquad (14)$$

where σ_r is the stress in the radial direction;

σ_θ is the stress in the tangential direction;

ϵ_r is the strain in the radial direction;

ϵ_θ is the strain in the tangential direction;

λ and μ are the Lamé parameters.

Classical equations of motion in the spherically symmetric case can be obtained in the coordinate system of interest in a direct manner by considering a small conical volume element described as follows: (1) A surface generated by a solid angle from a point in three space; (2) two concentric surface generated by radii with the aforementioned point as center. We assume the following symmetrical behavior:

1. The rate of change of momentum of the conical volume is equal to the total external force acting on the volume;
2. The mass of the moving volume remains unchanged under deformation of the medium.

In addition, we assume that the forces due to the acceleration of gravity can be neglected and that strains will be relatively small.

By further consideration of the elemental volume previously described, we can determine the relationship between the strain and the deformation. These relations are

$$\epsilon_r = \frac{\partial u_r}{\partial r} \quad , \qquad (15)$$

$$\epsilon_\theta = \frac{u_r}{r} \quad , \qquad (16)$$

where u_r is the radial deformation;

r is the radial distance.

In the classical fashion, we obtain the wave equation,

$$\frac{\partial^2 (r\psi)}{\partial t^2} = c^2 \frac{\partial^2 (r\psi)}{\partial r^2} \quad , \qquad (17)$$

when ψ is a displacement or velocity.

Where c is the velocity of sound in the medium and is given in terms of the Lamé constants and the density.[1]

$$c = \left(\frac{\lambda + 2\mu}{\rho} \right)^{1/2} .$$

In the case of small strains we can write the expression for the dilation as a linear function of the strain,

$$\Delta = \epsilon_\theta + 2\epsilon_\theta \qquad . \qquad (18)$$

and from Eqs. (15) and (16) we see that $r\Delta$ satisfies the wave equation. A solution to the wave equation is given by the arbitrary function $f[t - (r - b_o)/c]$. Equating this function to $r\Delta$ we have

$$r\Delta = f[t - (r - b_o)/c] \qquad , \qquad (19)$$

where b_o is the radial distance to the initial elastic boundary.

We may now write an equation which includes the deformation in the radial direction by substituting for the terms ϵ_r and ϵ_θ in Eq. (18) their equivalent forms given in Eqs. (15) and (16). After some manipulation we obtain the partial differential equation,

$$\frac{\partial}{\partial r}(r^2 u_r) - rf[t - (r - b_o)/c] = 0 \quad . \qquad (20)$$

For convenience we introduce a new function, F, given by the defining equation,

$$\frac{\partial^2}{\partial t^2} F[t - (r - b_o)/c] = f[t - (r - b_o)/c] \quad . \qquad (21)$$

---

[1] Thomas T. Y., Plastic Flow and Fracture in Solids, Academic Press (1961) p. 60 ff. Thomas also gives a more exact expression

$$c = \left[\frac{\rho}{\rho_o^2} (\lambda + 2\mu) \right]^{1/2}$$

where ρ is the density, a function of t and r.

We then form the integral of (20) incorporating the function, F, defined in Eq. (21) and after integration by parts obtain the differential equation,

$$-r^2 u_r = rc \frac{\partial}{\partial t} F[t - (r - b_o)/c] + c^2 F[t - (r - b_o)/c] \quad . \qquad (22)$$

Now, provided we know the boundary conditions for u_r, that is, if we know the deformation as a function of the time and the position of elastic boundary, we can determine the deformations for all time and radii. Similarly, we can obtain the particle velocity and particle acceleration for all time, t, at any radius, r, by differentiation of the expression for u_r obtainable from Eq. (22). In addition, substituting Eqs. (15) and (16) into Eq. (13) and using the relation just obtained for u_r in Eq. (22), we can determine for all time and radial distances, the radial stress wave, σ_r, which is propagating through the medium:

$$r^3 \sigma_r = \rho c^2 r^2 \frac{\partial^2 F}{\partial t^2} + 4\mu c r \frac{\partial F}{\partial t} + 4\mu c^2 F \quad . \qquad (23)$$

This equation can also be used to determine the function, F, provided we know the pressure versus time on the seismic boundary or else the pressure versus time at some other boundary.

Actually the boundary conditions required for Eqs. (22) and (23) may be obtained from the results of the computation carried out for wave propagation in a crushable media where we view the sequence of events as follows. The extremely high pressures generated within the bomb room at detonation time cause crushing of the soil out to some radial distance. Beyond this radius the waves propagate seismically. We may describe the crushed material as a large spherical piston which applies a force to the elastically responding soil

on its exterior. This spherical piston moves out to some maximum radius, all the while elastically deforming the soil on its exterior.

At this point in the discussion we must make some additional assumptions about the structural integrity of the thick walled spherical shell which makes up our piston. In general, we would expect that the structural integrity of this piston would be such that the elastic response of the surrounding soil would tend to drive the spherical piston back towards the center of the cavity until the force due to the cavity pressure and the restraining force due to the residual structural integrity of the spherical shell becomes sufficient to balance the static stress applied by the surrounding soil. Perhaps one might also expect mechanical oscillation of this spherical piston as a consequence of the elastic properties of the solid constituent of the crushed material.

For purposes of computation we assume the following: the pressure exerted by the spherical piston on the surrounding elastic material is subject to a step rise after which the pressure relaxes gradually. This would be similar to the effect we would have if our spherical piston deformed the surrounding material to some maximum value and then partially relaxed, maintaining a quasi-static stress level and therefore a permanent deformation. In order to determine some qualitative wave shapes, a solution was obtained for Eq. (23). The solution function is given by Eq. (23) where the function

F is[2]

$$F(t) = e^{-aT}(A \sin bT + B \cos bT) + \frac{1}{b}\int_0^T f(\tau)e^{a(\tau - T)/2}\sin b(T - \tau)d\tau \quad ; \quad (24)$$

where $a = 2\mu/b_o\rho c$

$$b = 2[\mu(\lambda + \mu)]^{1/2}/b_o\rho c$$

$$T = t - (r - b_o)/c$$

$$f(\tau) = b_o P(\tau, b_o)/\rho c^2$$

A and B are constants determined by the initial data. Particular solutions of Eq. (23) have previously been obtained by Selberg[3], Goldsmith and Allan[4], and others.

We note from the particle velocity plots of the more distant hypothetical velocity gages, which were considered in Section II, that the character of the wave can be approximated by an exponential decay with a long time constant. For

---

[2]Kamke, E., Differentialgleichungen Lösungsmethoden Und Lösungen, Chelsea Publishing Company, New York, 1959, pp. 412, 413.

[3]Selberg, Henrik L., "Transient Compression Waves from Spherical and Cylindrical Cavities," Arkiv För Fysik, Vol. 5, Stockholm, 1952, p. 97 ff.

[4]Goldsmith, W. and Allan, W. A., "Graphical Representation of the Spherical-Propagation of Explosive Pulses in Elastic Media," Journal of Acoustical Society of America, Vol. 27, pp. 47-55, 1955.

seismic disturbances we have approximately

$$P = \rho c v \quad ; \qquad (25)$$

where P = pressure;

ρ = the density of the soil;

c = propagation velocity;

v = particle velocity.

and this implies that the pressure on the boundary between the permanently crushed and seismic regions can be approximated by

$$P = P_o e^{-t/\tau} \quad ; \qquad (26)$$

where τ is determined using Eqs. (25) and (26) and the data obtained in Sec. II for the particle velocity;

P_o is the peak pressure and is determined from Eq. (25) and the data of Sec. II.

We now set

$$P = -\sigma_r(b_o, t) \quad ; \qquad (27)$$

where $\sigma_r(b_o, t)$ is the stress in the radial direction at the elastic boundary. Substitution of this into Eq. (24) determines the function, F, which upon substitution into Eq. (22) yields an expression for the deformation. Subsequent differentiations yield expressions for the particle velocity and acceleration.

Computations were carried out to determine displacement, velocity, and acceleration wave forms. Two sets of these computations are shown. One set was obtained using the elastic constants measured for salt, and the other used average values measured for tuff. The required input data is:

1. Young's modulus, E;
2. Poisson's ratio, υ;

3. Density, ρ;

4. Peak boundary particle velocity;

5. Time constant, τ;

6. Range to hypothetical gage, r;

7. Radial distance to the seismic boundary, b_o.

We note that at the wave front the peak particle velocity falls off as 1/r. Similarly, the deformation falls off as 1/r in the case of dynamic loading but as $1/r^3$ in the case of static loading. The displacement rises rapidly to a peak value, then recedes and tends to oscillate about some steady state value but damps out rapidly.

Figs. 11, 12, and 13 show the displacement, velocity and acceleration as a function of time at a hypothetical gage 300 ft. from the explosive source. The constants used to describe the mechanical behavior of the soil are those measured for tuff. Figs. 14, 15, and 16 show similar curves for the disturbance as measured at a hypothetical gage 900 ft. from the explosive source. Figs. 17 through 22 are a set of figures similar to 11 through 16, but indicate the wave shapes where the propagation medium is salt. A comparison of these two sets of wave forms indicates that those for tuff contain lower frequency components than the similar ones for salt. Also, the displacements in salt are smaller than in tuff. These facts partially explain the reason for shots in tuff being more easily detected at a distant station than the same yield shot in salt.

Fig. 23 shows the displacement wave measured at the 298 meter station in the GNOME event. The character of the wave is similar to that predicted analytically.

Fig. 24 shows the shape of elastic displacement waves generated by mechan-

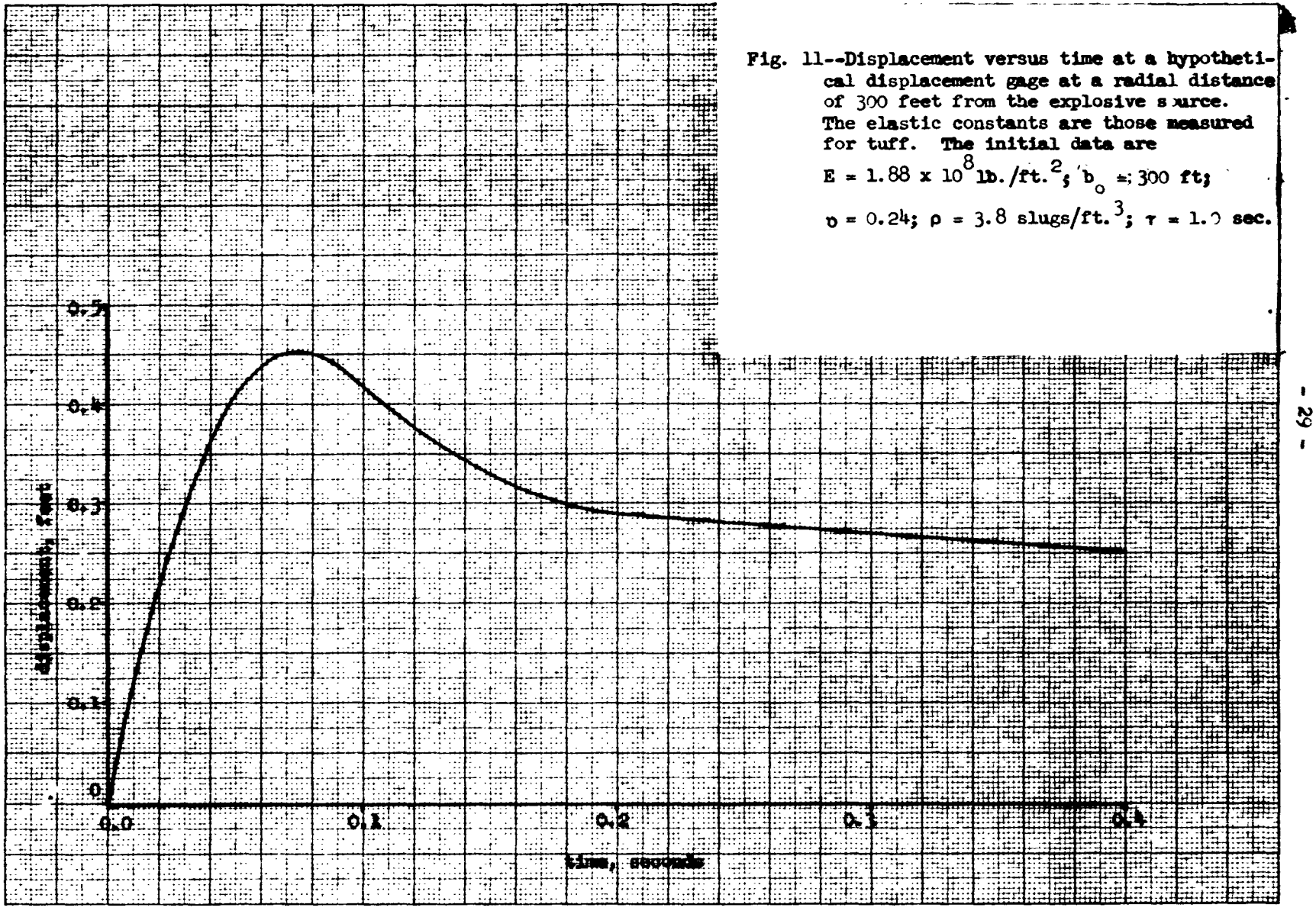

Fig. 11--Displacement versus time at a hypothetical displacement gage at a radial distance of 300 feet from the explosive source. The elastic constants are those measured for tuff. The initial data are

$E = 1.88 \times 10^8$ lb./ft.^{2}; $b_o = 300$ ft;

$\upsilon = 0.24$; $\rho = 3.8$ slugs/ft.^{3}; $\tau = 1.0$ sec.

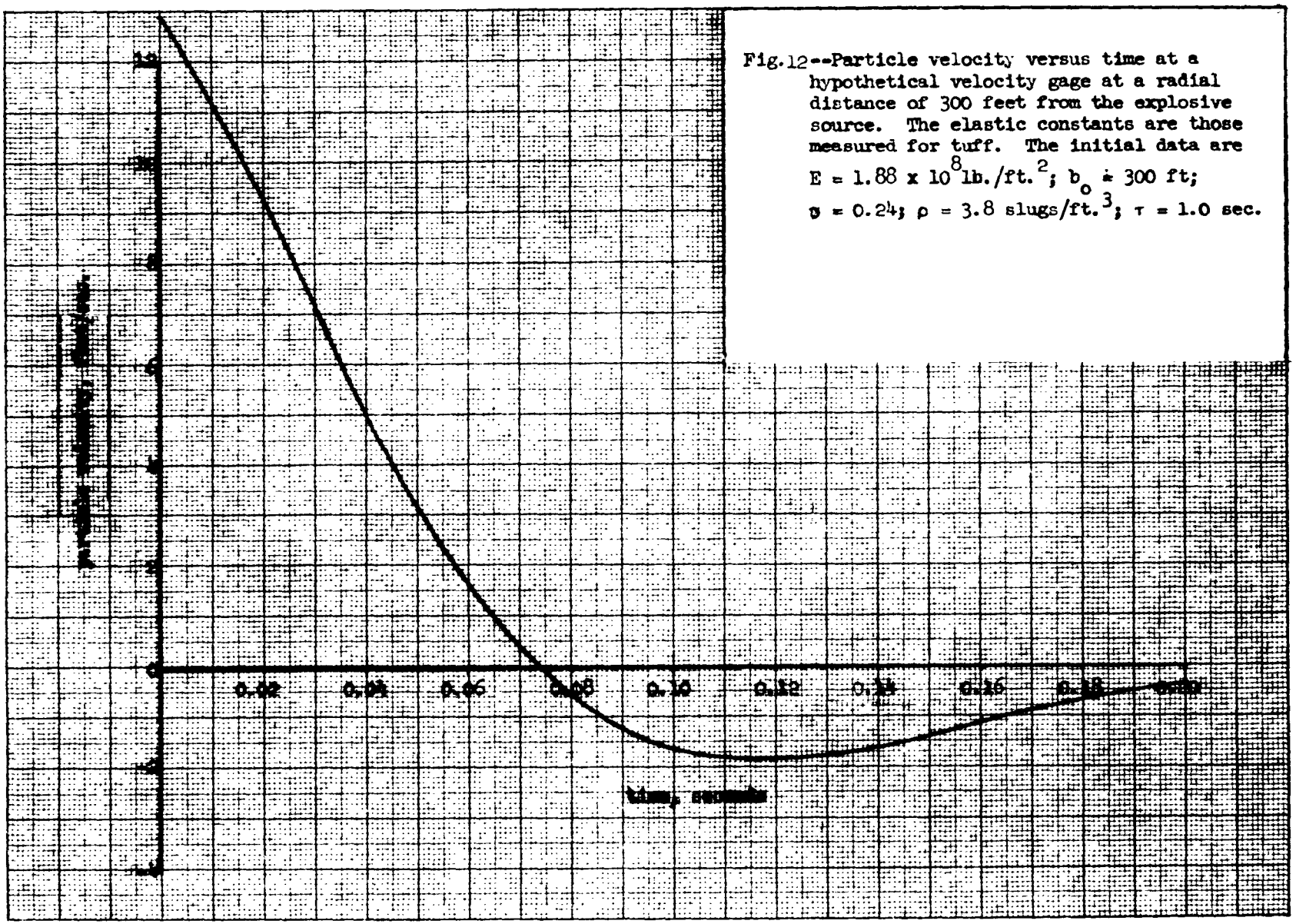

Fig. 12--Particle velocity versus time at a hypothetical velocity gage at a radial distance of 300 feet from the explosive source. The elastic constants are those measured for tuff. The initial data are $E = 1.88 \times 10^8$ lb./ft.^{2}; $b_o = 300$ ft; $\sigma = 0.24$; $\rho = 3.8$ slugs/ft.^{3}; $\tau = 1.0$ sec.

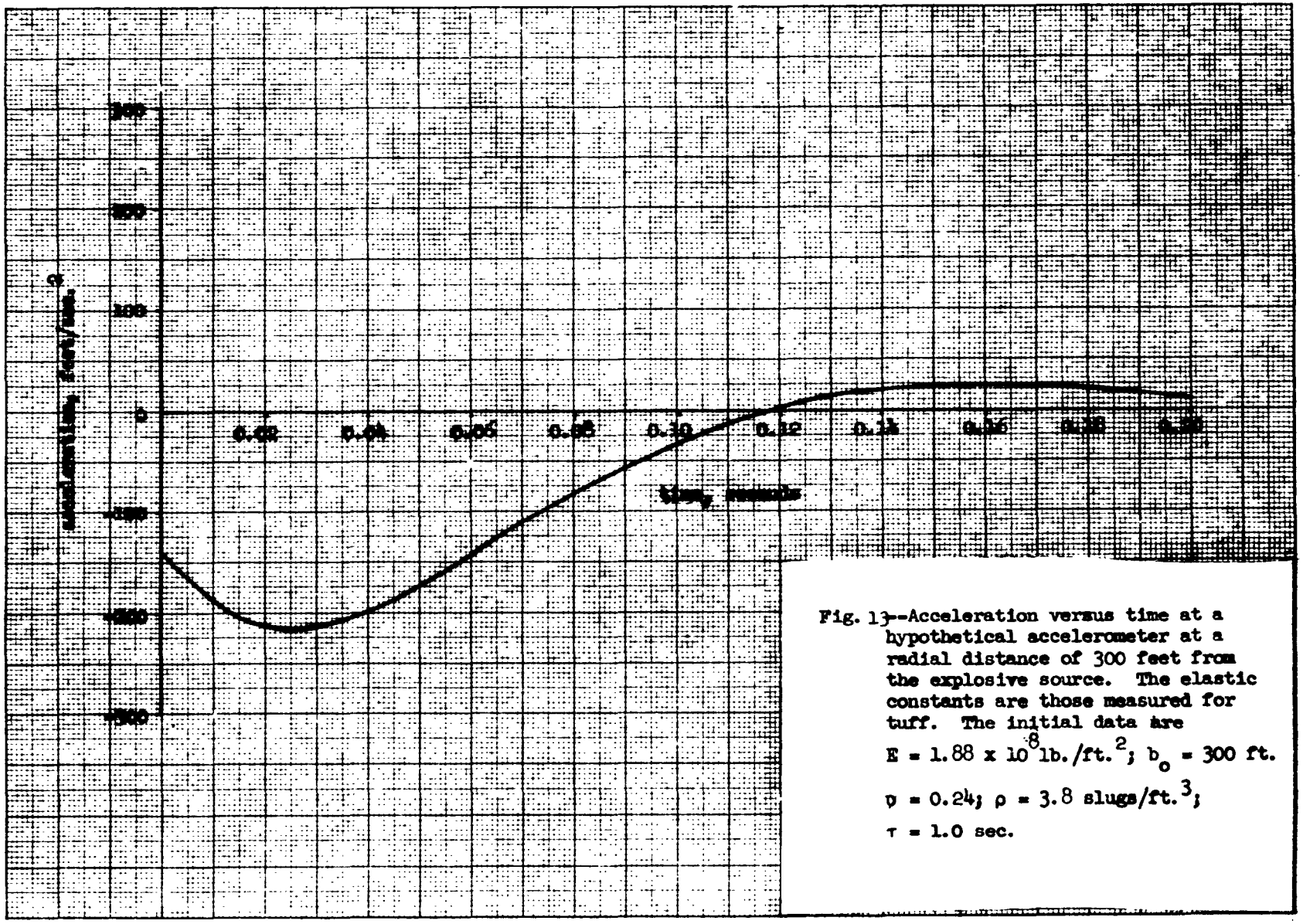

Fig. 13--Acceleration versus time at a hypothetical accelerometer at a radial distance of 300 feet from the explosive source. The elastic constants are those measured for tuff. The initial data are $E = 1.88 \times 10^{8}$ lb./ft.^{2}; $b_o = 300$ ft. $\nu = 0.24$; $\rho = 3.8$ slugs/ft.^{3}; $\tau = 1.0$ sec.

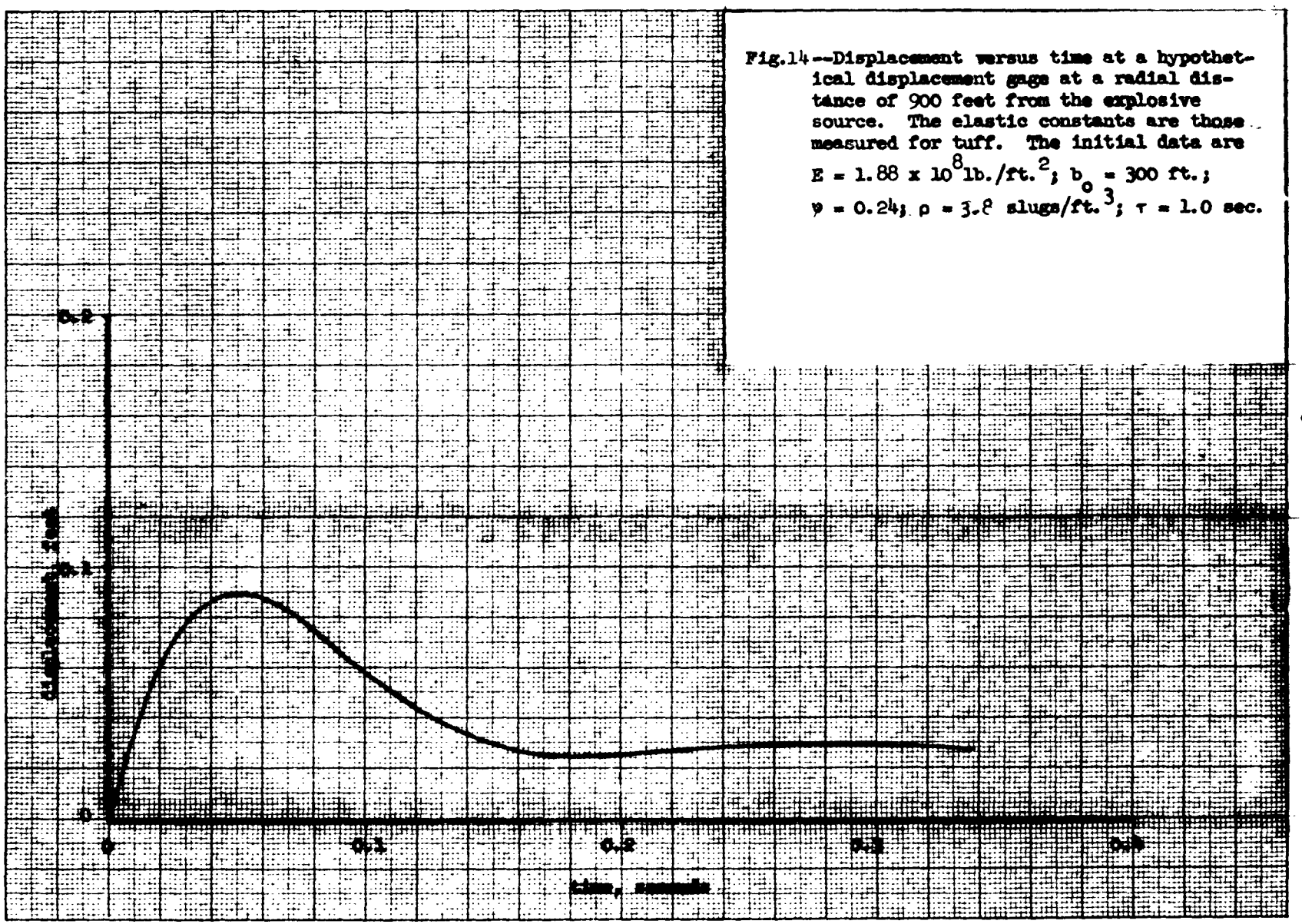

Fig.14--Displacement versus time at a hypothetical displacement gage at a radial distance of 900 feet from the explosive source. The elastic constants are those measured for tuff. The initial data are $E = 1.88 \times 10^8$ lb./ft.^{2}; $b_o = 300$ ft.; $\nu = 0.24$; $\rho = 3.8$ slugs/ft.^{3}; $\tau = 1.0$ sec.

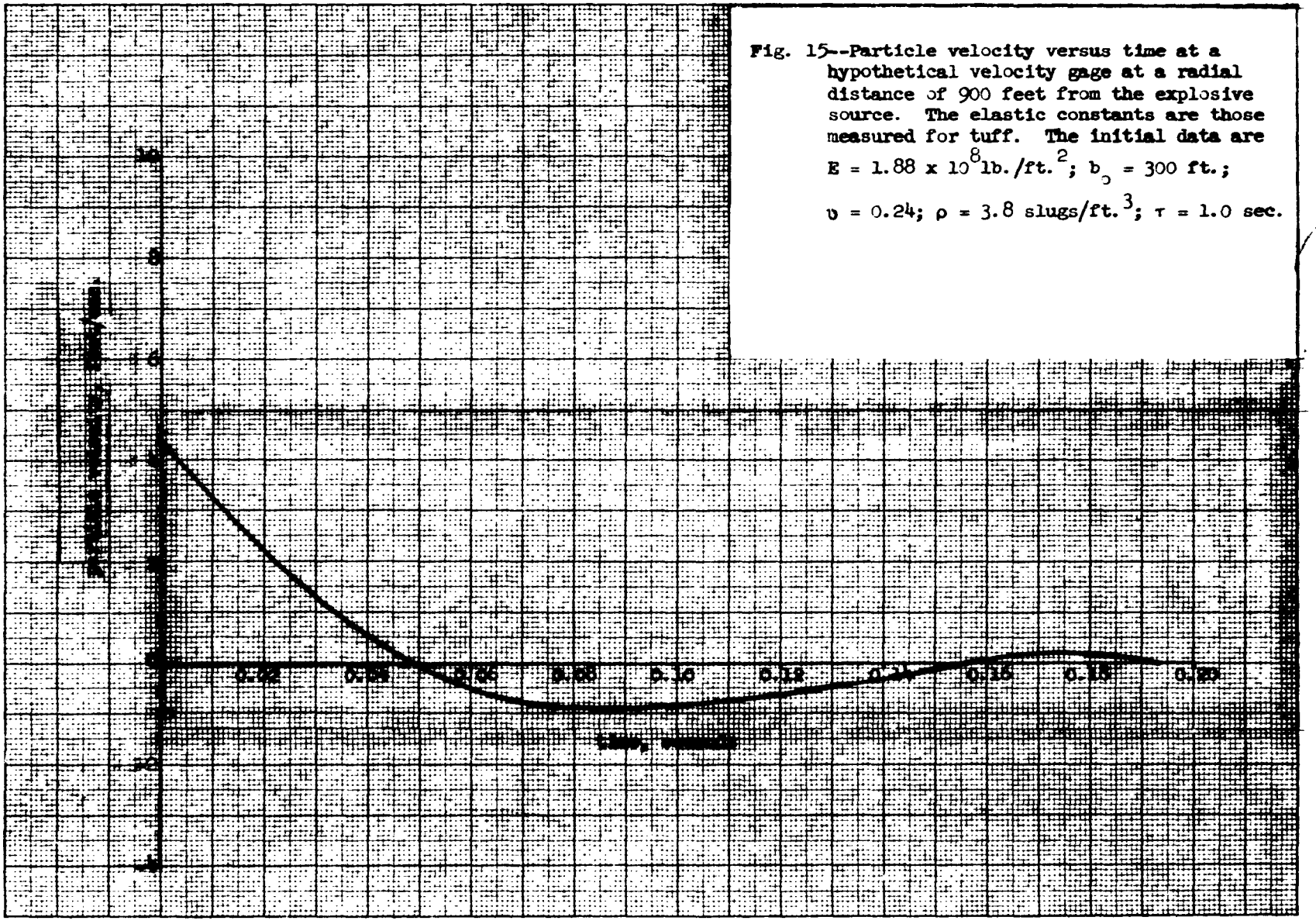

Fig. 15--Particle velocity versus time at a hypothetical velocity gage at a radial distance of 900 feet from the explosive source. The elastic constants are those measured for tuff. The initial data are $E = 1.88 \times 10^{8}$ lb./ft.^{2}; $b_{\circ} = 300$ ft.; $\upsilon = 0.24$; $\rho = 3.8$ slugs/ft.^{3}; $\tau = 1.0$ sec.

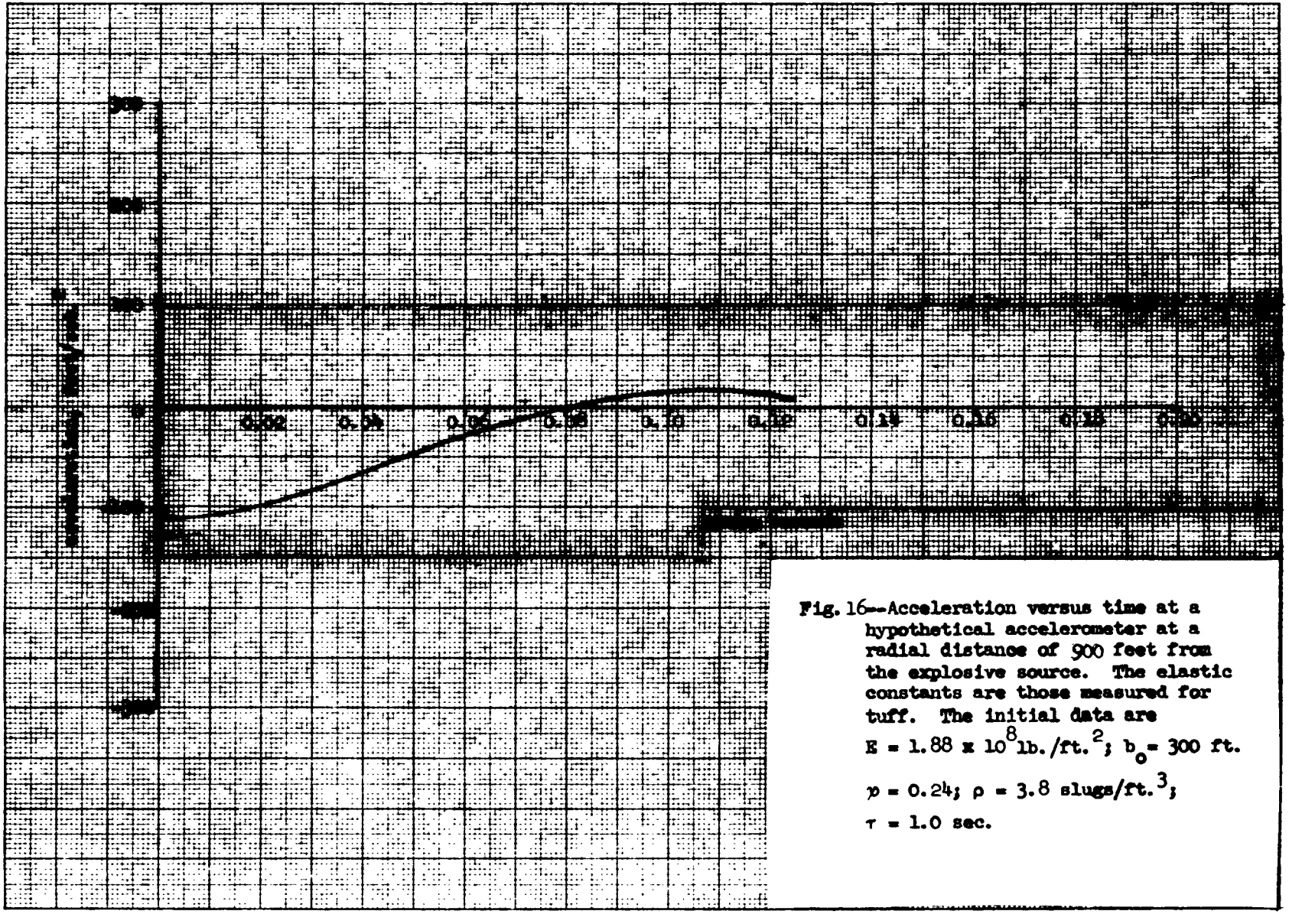

Fig. 16--Acceleration versus time at a hypothetical accelerometer at a radial distance of 900 feet from the explosive source. The elastic constants are those measured for tuff. The initial data are $E = 1.88 \times 10^8$ lb./ft.^{2}; $b_o = 300$ ft. $\nu = 0.24$; $\rho = 3.8$ slugs/ft.^{3}; $\tau = 1.0$ sec.

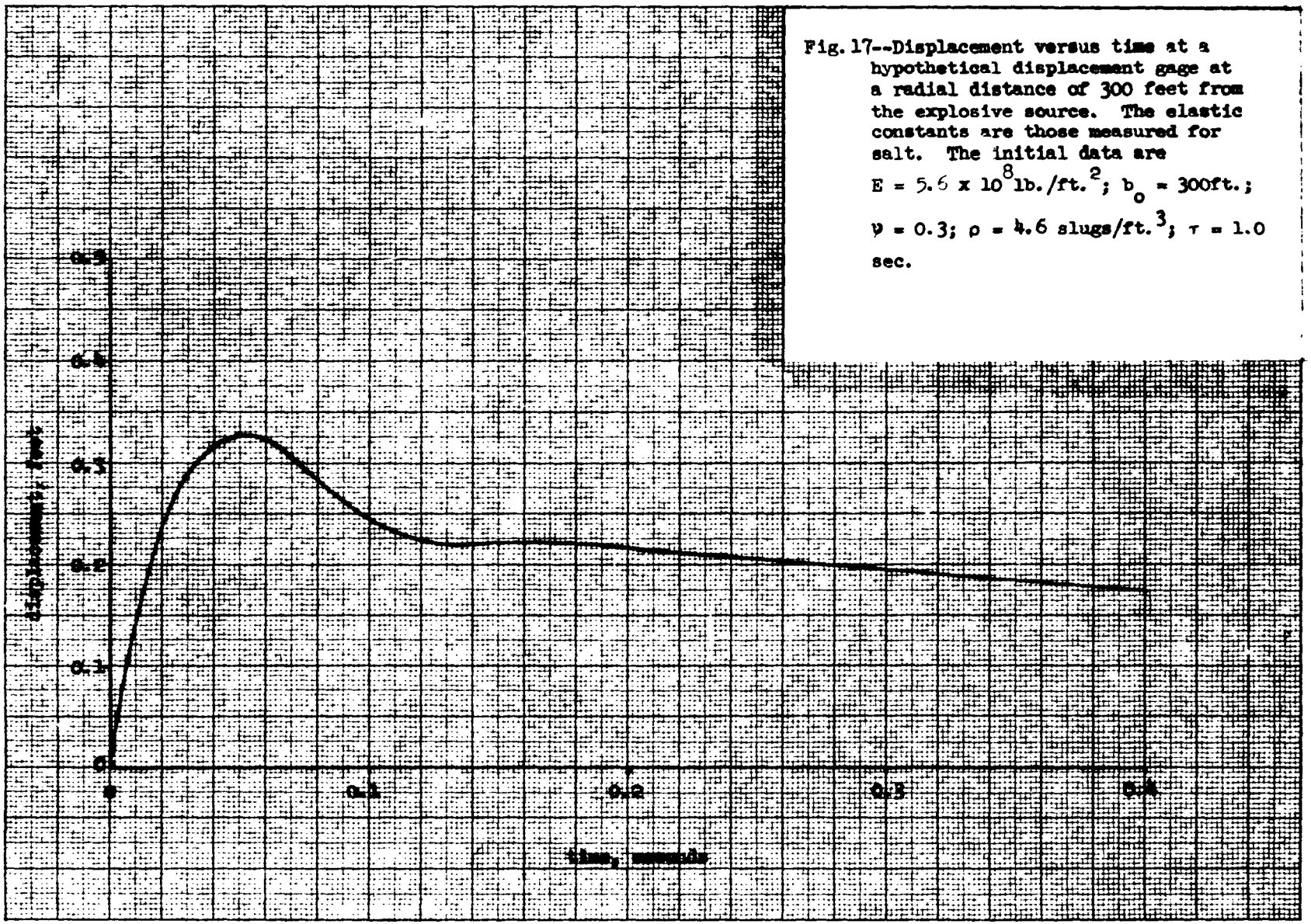

Fig. 17--Displacement versus time at a hypothetical displacement gage at a radial distance of 300 feet from the explosive source. The elastic constants are those measured for salt. The initial data are $E = 5.6 \times 10^8$ lb./ft.^{2}; b_o = 300ft.; $\nu = 0.3$; $\rho = 4.6$ slugs/ft.^{3}; $\tau = 1.0$ sec.

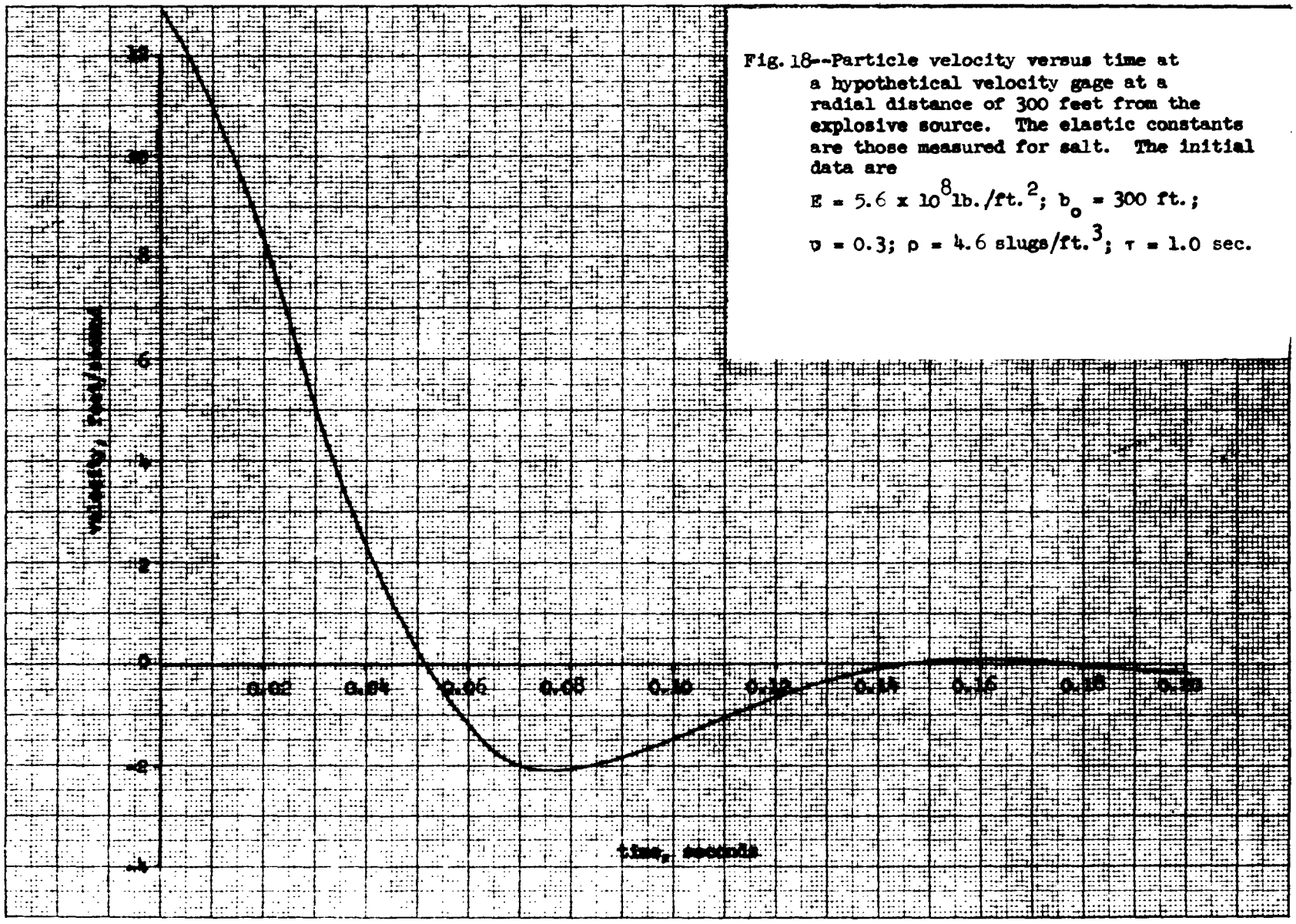

Fig. 18--Particle velocity versus time at a hypothetical velocity gage at a radial distance of 300 feet from the explosive source. The elastic constants are those measured for salt. The initial data are

$E = 5.6 \times 10^8$ lb./ft.^{2}; $b_o = 300$ ft.;

$\upsilon = 0.3$; $\rho = 4.6$ slugs/ft.^{3}; $\tau = 1.0$ sec.

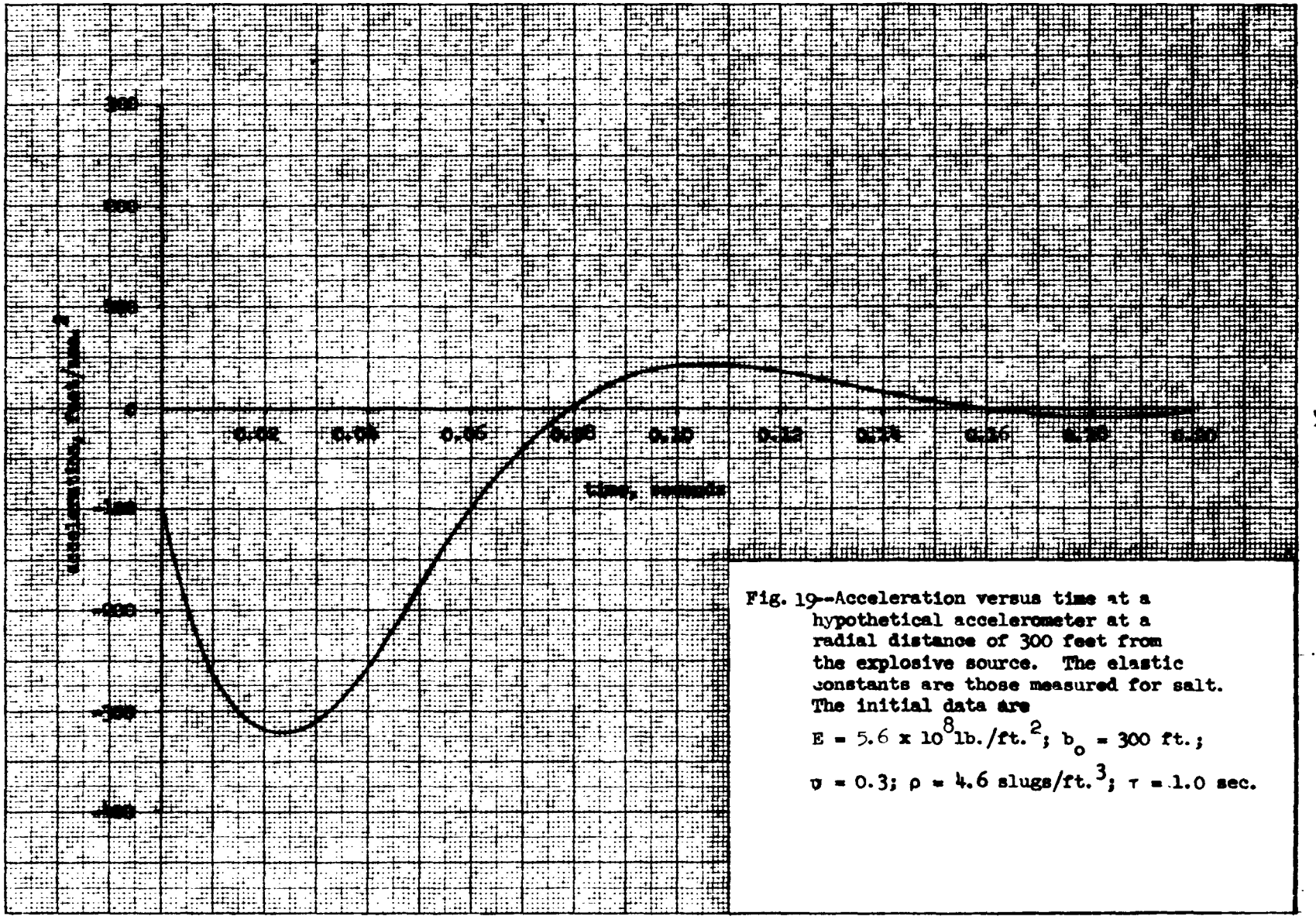

Fig. 19--Acceleration versus time at a hypothetical accelerometer at a radial distance of 300 feet from the explosive source. The elastic constants are those measured for salt. The initial data are

$E = 5.6 \times 10^8$ lb./ft.^{2}; $b_o = 300$ ft.;

$\upsilon = 0.3$; $\rho = 4.6$ slugs/ft.^{3}; $\tau = 1.0$ sec.

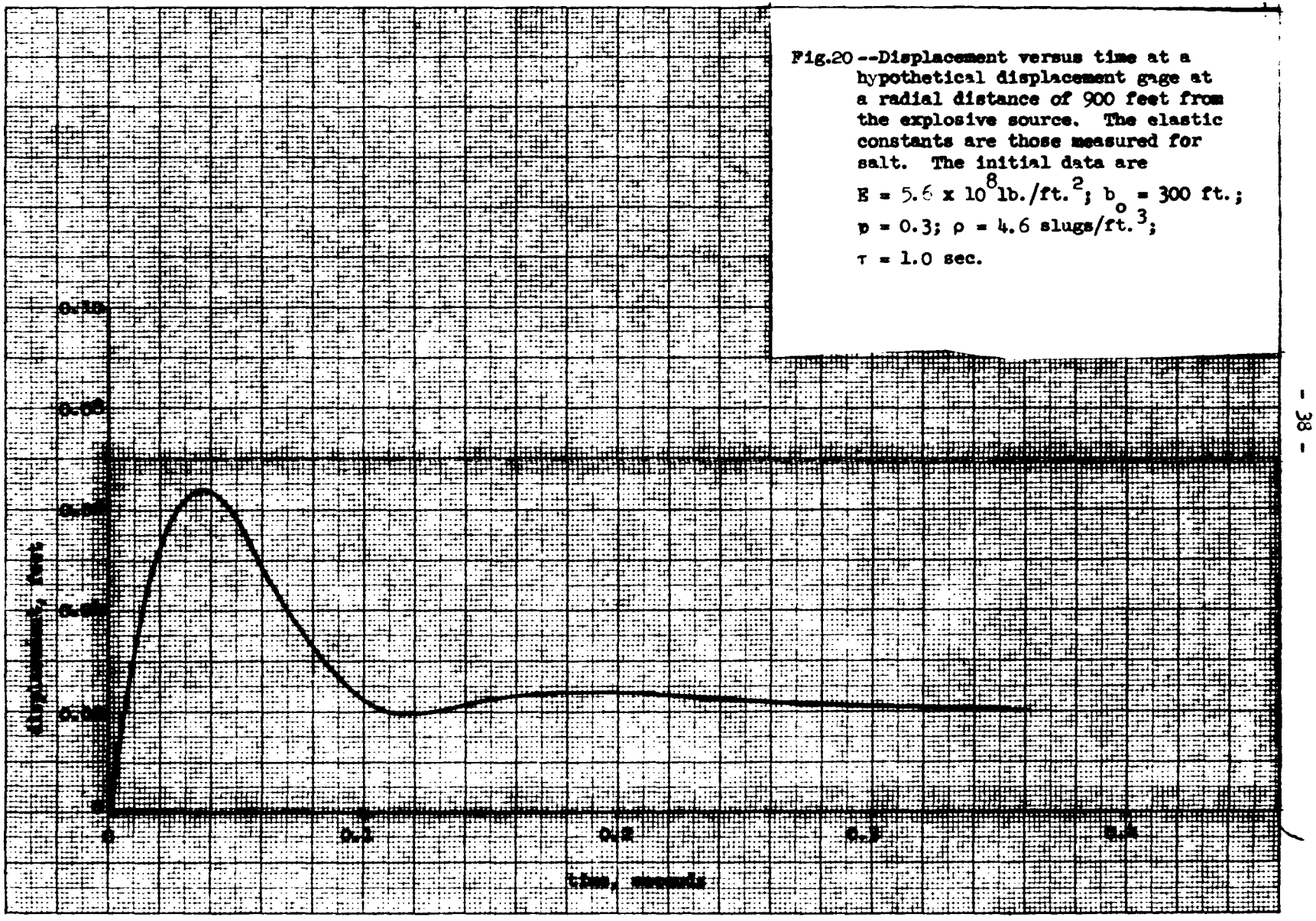

Fig.20 --Displacement versus time at a hypothetical displacement gage at a radial distance of 900 feet from the explosive source. The elastic constants are those measured for salt. The initial data are $E = 5.6 \times 10^8$ lb./ft.^{2}; $b_o = 300$ ft.; $p = 0.3$; $\rho = 4.6$ slugs/ft.^{3}; $\tau = 1.0$ sec.

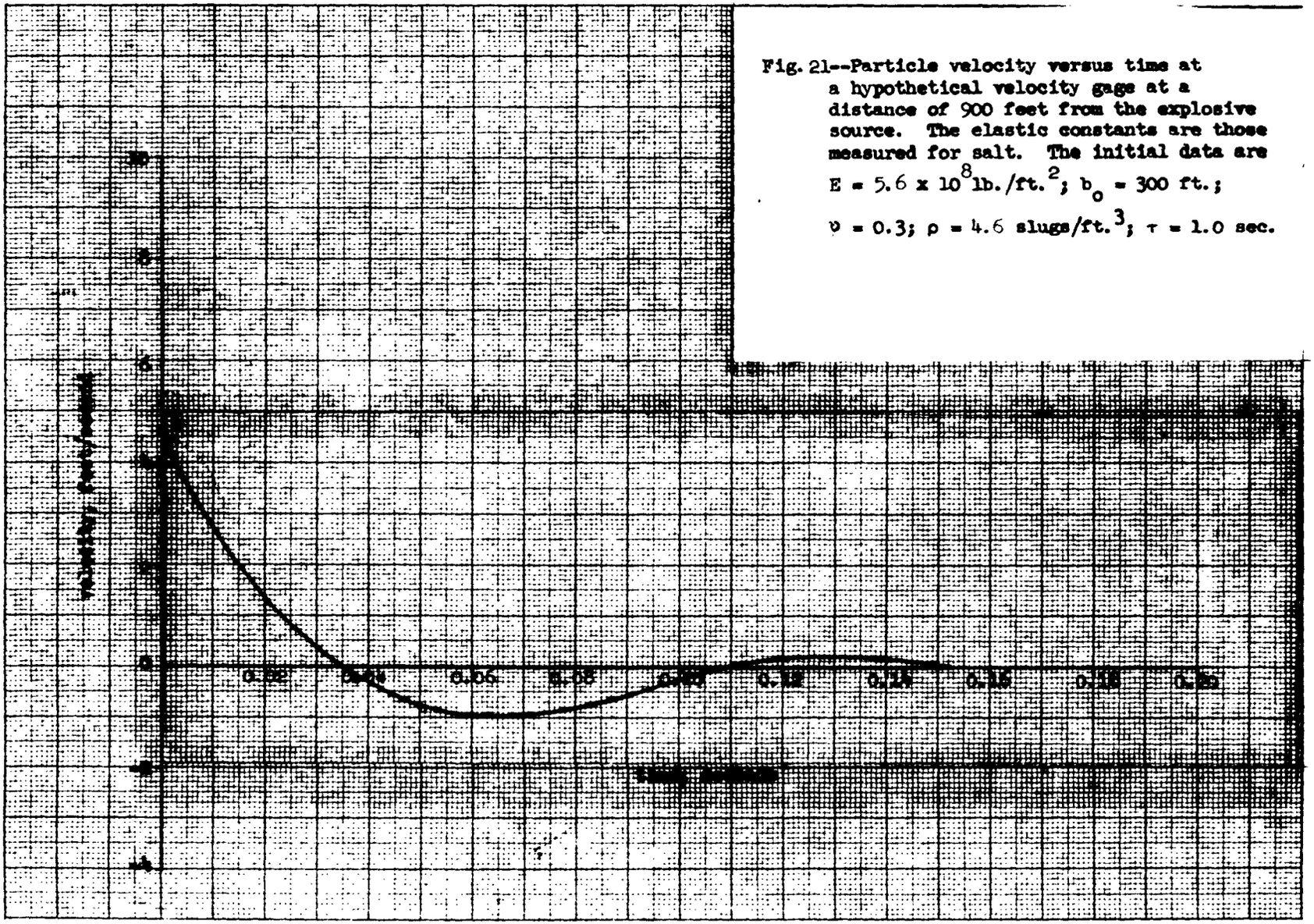

Fig. 21--Particle velocity versus time at a hypothetical velocity gage at a distance of 900 feet from the explosive source. The elastic constants are those measured for salt. The initial data are $E = 5.6 \times 10^8$ lb./ft.^{2}; $b_o = 300$ ft.; $\nu = 0.3$; $\rho = 4.6$ slugs/ft.^{3}; $\tau = 1.0$ sec.

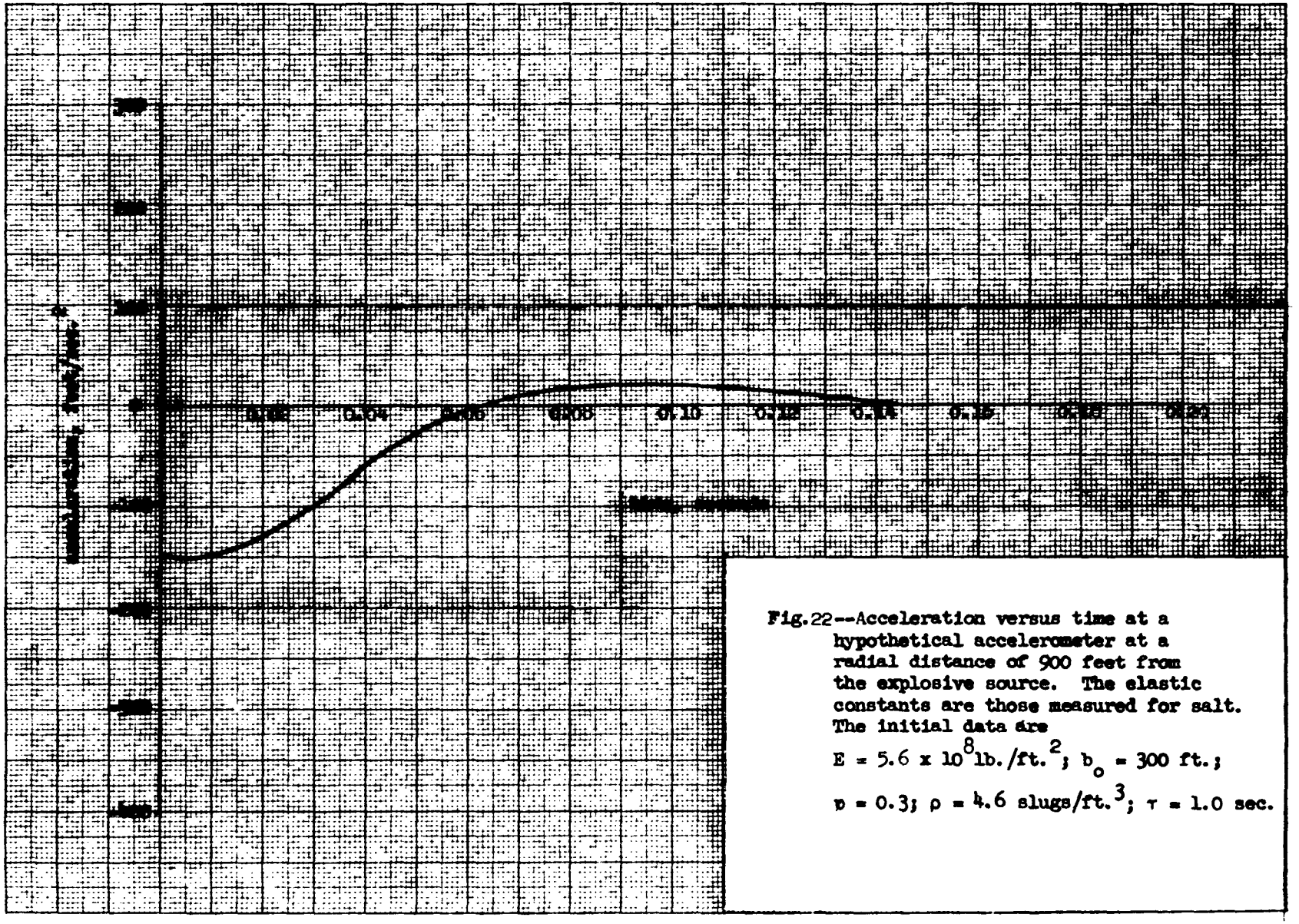

Fig. 22--Acceleration versus time at a hypothetical accelerometer at a radial distance of 900 feet from the explosive source. The elastic constants are those measured for salt. The initial data are

$E = 5.6 \times 10^8$ lb./ft.^{2}; $b_o = 300$ ft.;

$\nu = 0.3$; $\rho = 4.6$ slugs/ft.^{3}; $\tau = 1.0$ sec.

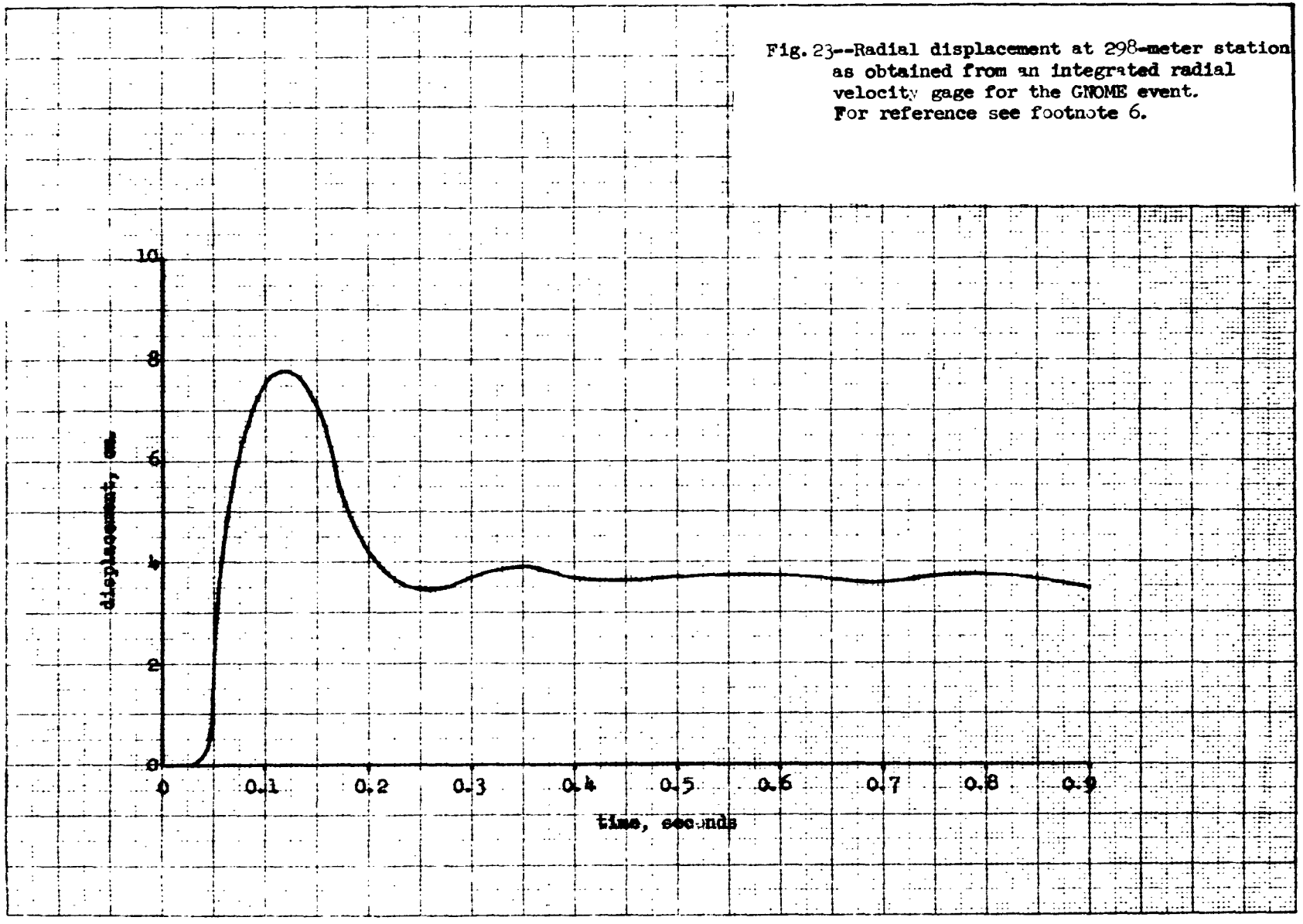

Fig. 23--Radial displacement at 298-meter station as obtained from an integrated radial velocity gage for the GNOME event. For reference see footnote 6.

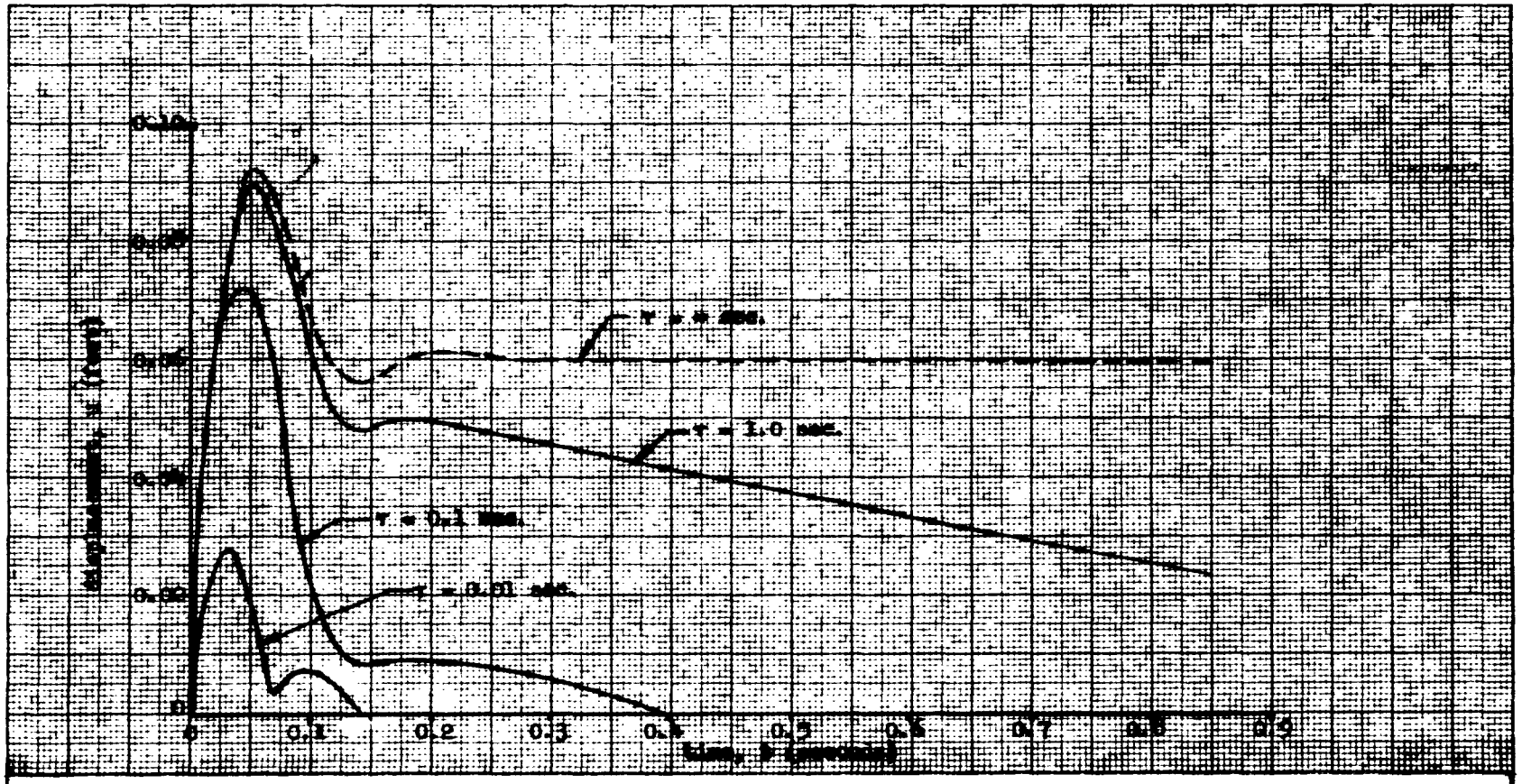

Fig. 24--Radial distance of 500 feet from the explosive source. Plots are shown for several different values of the time constant, τ.

ical disturbances having various time constants. For a contained explosion, the time constants are generally long as indicated by the analysis of Section II; however, in the case of early and rapid venting of the cavity, the time constant may be rather short.

IV. ELASTIC PRECURSOR

A so-called elastic precursor has been observed in laboratory[5] scale wave propagation experiments using naturally occuring earth materials. Additionally, there are some large scale experimental records[6] which indicate to some extent the existence of a precursor. Indeed, one would expect a precursor on theoretical grounds[7], since experimental evidence shows that the shock wave, while propagating through soil near the source of the explosion, can vary in velocity from supersonic to subsonic and back to sonic. During the time the shock front is propagating subsonically, we would expect a sonic disturbance to propagate ahead with an amplitude determined by the maximum elastic energy which can be contained in the earth material under consideration. Actually, the amount of elastic energy which can be stored in a given mass of earth material is subject to change dependent on the length of time the energy is stored. Hence, the magnitude of the disturbance which is propagated through the soil depends on the soil's stress-strain history. For the moment, we will neglect this latter fact and set up some simple relations to describe the precursor in terms of:

---

[5] Chabai, A. J., "Research and Analysis of Close-In Data," Contract No. DASA-EO-300-60, Semiannual Report, May 1, 1961 - October 1, 1962, Sandia Corporation Project No. 14.041.00.

[6] Weart, W. D., "Particle Motion Near A Nuclear Detonation in Halite," Project GNOME, PNE-108, Sandia Corporation, Preliminary Report, Projects 44.1 and 1.1, Feb. 1962.

[7] Nuckolls, John H., "A Computer Calculation of Rainier," Lawrence Radiation Laboratory, Livermore, PLOWSHARE SERIES, Part I, Phenomenology of Underground Nuclear Explosions, UCRL-5675, May 13-15, 1959.

1. The velocity history of the shock front;
2. An assumed peak pressure, P_o, for elastic waves in the medium under consideration.

We take the shock front velocity to be $\dot{R}$ and the position of the shock front at time, t, to be R.

In the acoustic approximation, spherical divergence prescribes that the peak pressure be inversely proportional to r, the radial distance from the point of emission. We assume that the pressure, P_o, is the maximum allowable pressure which can be propagated acoustically in the medium. Let τ be any time during which an acoustic disturbance is emitted from the traveling shock front. A typical plot of time versus shock front velocity would have the form shown in Fig. 25. Then the position, r_p, of the precursor wave front at some time, t, where $t \geq \tau$, is given by

$$r_p = R(\tau) + (t - \tau)c \quad , \tag{28}$$

where c is the sonic velocity in the medium.

Therefore, at this time, t, the pressure, P, of the emitted disturbance is given by (in the acoustic approximation)

$$P = \frac{P_o R(\tau)}{r_p} \quad . \tag{29}$$

Using the acoustic approximation

$$P = \rho c v \quad , \tag{30}$$

where ρ is the density of the medium

v is the particle velocity in the medium

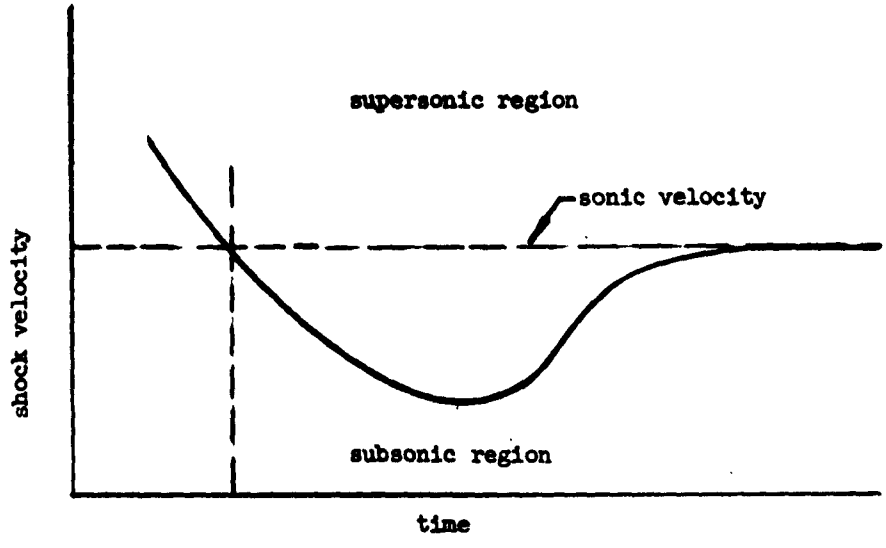

Fig. 25--A typical shock velocity versus time plot showing supersonic, subsonic and sonic phases of shock wave propagation.

we have

$$v = \frac{v_o R(\tau)}{r_p} \quad , \qquad (31)$$

where $v_o = P_o/\rho c$

Combining this result with Eq. (28) yields

$$v = \frac{v_o R(\tau)}{R(\tau) + (t - \tau)c} \quad . \qquad (32)$$

Now, at a particular gage located at a distance, r_g, from the explosive source, and at a time, t, we have from Eq. (28)

$$t = \frac{r_g - R(\tau)}{c} + \tau \quad . \qquad (33)$$

Knowing the position of the shock front as a function of time from an analysis such as that given in Section II or from experimental data we can vary the parameter, τ, and determine from Eqs. (32) and (33), the particle velocity as a function of time.

For $t > \tau$ the particle velocity history of the existing wave is as shown in Fig. 26.

The pressure at the leading edge of the elastic precursor is smaller than that at the shock front due to the 1/r fall off assumed in the acoustic approximation.

However, there is yet another phenomenon which affects the wave form: namely, the relaxation of the medium after passage of the precursor wave front. This is a property of the medium under consideration, but, in general, the stress is relieved internally in the medium and thus the particle velocity decreases behind the precursor wave front as illustrated in Fig. 27. A somewhat similar behavior

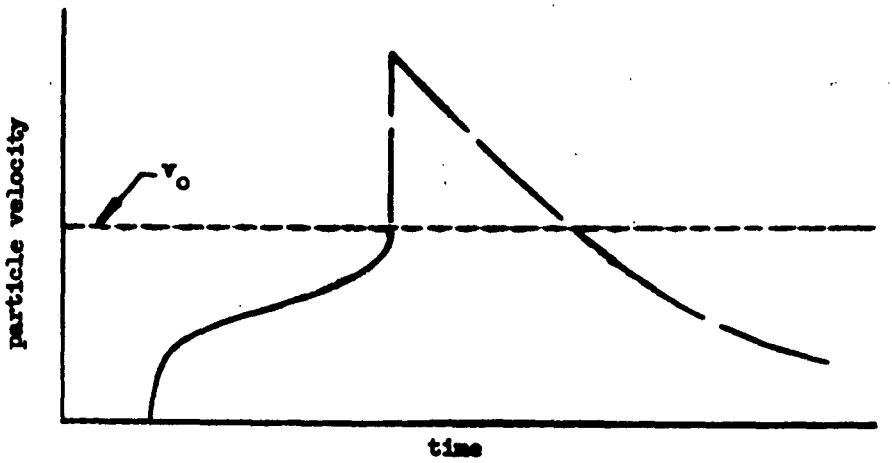

Fig. 26--Precursor is indicated by solid curve. Main shock wave is shown by broken curve. Curves are not necessarily to scale since precursor may be of short duration compared to main disturbance.

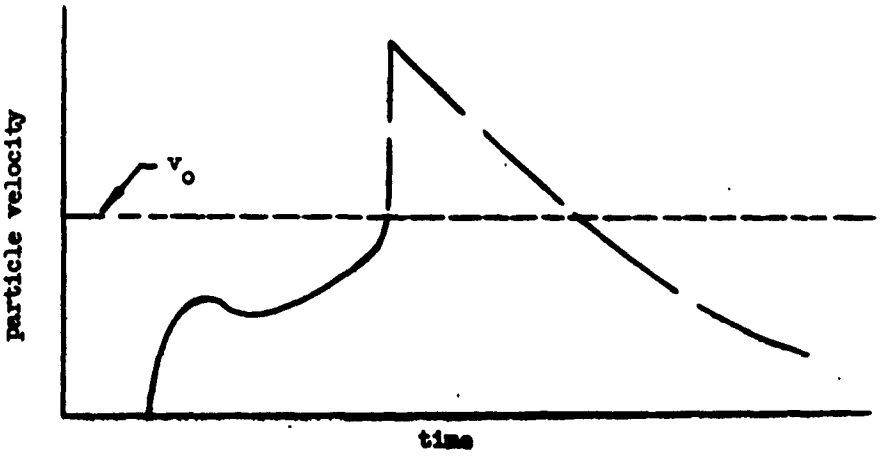

Fig. 27--The effect of the relaxation phenomenon on the initial precursor wave form.

can be noted in the case of elastic waves previously described in Section III.

The distance between the precursor wave front and the shock front lengthens when $\dot{R} < c$, but when the shock front velocity increases to sonic velocity, the distance between the fronts remains fixed, with the shock particle velocity dropping to v_o, and hence not distinct from the rest of the wave form. Therefore, the final wave form that propagates elastically into the medium has the form given by Fig. 28.

In the event that the shock front velocity drops only slightly below the acoustic velocity of the soil or in the event the shock front velocity is subsonic for only a short time the precursor may not be detected by gages that are used primarily to detect the entire wave. Many field records give no indication of a precursor suggesting that the gage did not respond to the precursor or else that the precursor in some cases simply does not exist.

Gages having the proper response characteristics might be used to obtain information about the soil behavior near the source of an explosion. For example, if we know the particle velocity as a function of time at a gage a known distance from the explosive source, as well as the density, velocity of propagation, and the maximum pressure of elastic waves, then one can determine from Eqs. (30), (31) and (33) the new equations

$$R(\tau) = \frac{\rho c v(t) r_g}{P_o} \quad , \qquad (34)$$

$$\tau = t - \frac{r_g - R(\tau)}{c} \quad , \qquad (35)$$

which yield the required shock wave velocity as a function of time.

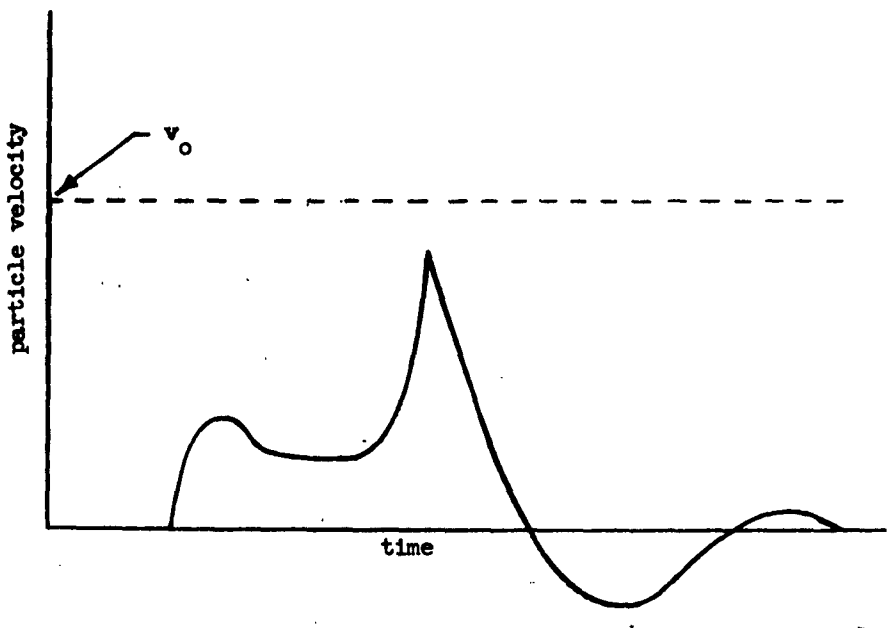

Fig. 28--Final wave form after main disturbance begins to propagate elastically. Precursor may be of considerably shorter duration compared to the direct disturbance than is indicated here.

If we had records from several gages they could be used to obtain a best fit for the shock wave position and velocity as a function of time or else for each additional gage we could determine one of the before required inputs such as density or propagation velocity of the soil.

Furthermore with data describing the position of the shock front and its velocity as a function of time we can use an analysis somewhat the reverse of that given in Section II and thereby determine important information about the equation of state of the soil near the explosive source.

V. SPALLING AND SECONDARY WAVES

Spalling of the earth may result as a secondary effect of an underground nuclear explosion. The following mechanism is the cause of spalling: the initial shock wave generated by the explosive source propagates towards the earth's surface and upon interaction with the surface, generates a rarefaction wave which begins to propagate back into the soil, having the effects of increasing the particle velocity in the direction normal to the surface and at the same time relieving the compressive stress of the tail of the direct pressure wave. At some depth the sum of: (1) the stress of the tail of the direct wave; (2) the lithostatic stress; and, (3) the tensile stress of the rarefaction wave, may represent a tensile force in excess of that required for rupture of the soil. At this instant and at this depth, rupture will occur and the slab defined by the fractured surface and the earth's surface will be hurled upward. There has been ample experimental evidence of surface behavior of this sort.

Spalling has evidenced itself in the records of vertical accelerometers placed in the soil above underground nuclear explosions. For example, in the Rainier shot, an acceleration of one gravity was measured by near surface gages for a period of about 1/2 second, indicating that soil was being acted upon essentially by gravity alone during that period. Such behavior was noted on gages buried at depths of 200 to 250 feet below the surface, suggesting that rupture took place beneath this depth.

From the VELA-UNIFORM point of view, secondary wave generation which results from spalling can be of considerable importance, since a large amount of propagated

energy may be trapped in the massive slab of spalled earth which eventually impacts the underlying earth, generating the observed secondary waves. Depending upon the geometric configuration of the spalled slab and the underlying surface it impacts, this energy may represent a large fraction of the hydrodynamic energy produced by an underground nuclear explosion. The waves generated in this fashion contain valuable information about the close-in soil characteristics, the wave shape of the direct wave close-in, the depth of burst, and the yield. Since these waves follow the direct waves by a considerable length of time, perhaps in the order of one second or more, the two wave forms can be distinguished. By correlation of these two types of waves, it may be possible to extract information about the mechanism of their generation.

In the literature, one can find numerous papers dealing with the mechanism of spalling; however, not a great deal of information exists which describes secondary wave generation. A phenomenon akin to spalling in the case of underwater explosions is called bulk cavitation. In this case, there has been some investigation of the generation of secondary waves, in addition to some experiments to study the phenomenon.[8] EPCO is presently carrying out a theoretical investigation of a three-dimensional bulk cavitation problem for the Office of Naval Research.[9] Because of the similarity between the mechanism of spalling and that of bulk cavitation, we find that we may use similar mathematical models to explain qualitatively

---

[8] Tests conducted in June, 1962 by Underwater Explosions Research Division of the David Taylor Model Basin.

[9] Contract NONr-3709(00)

the type of secondary waves which are emitted in either case. Some of the basic differences which are evident when the medium under consideration is soil rather than water, are enumerated below:

1. Existence of shearing forces;
2. Non-homegeneity;
3. Relatively large compressibility.

In the latter portion of this section, we will undertake a rudimentary analysis of secondary wave generation in soil.

For purposes of our simplified mathematical model, we will make the following assumptions:

1. The earth's surface is completely flat and horizontal in the neighborhood of the explosive source;
2. The soil is homogeneous and isotropic;
3. The propagation velocities of both compression and tension waves are identical;
4. The primary wave shape has a sharp rise and an exponential tailoff;
5. The maximum tensile strength of the soil is a known constant;
6. The amplitude of the shear waves are negligibly small compared to that of the direct compression.

While the conditions just assumed are rather restrictive, our model should describe qualitatively the features of the secondary waves actually generated.

It is instructive at the outset to consider the tension field which exists when spallation does not occur. By considering the sum of the direct stress wave,

lithostatic pressure, and the tensile stress caused by the rarefaction wave in a three-dimensional situation where the explosive source is considered a point source, we obtain various typical stress fields where the tensile stress is equal to or in excess of the maximum tensile strength of the soil. The shape of field is dependent upon the wave shape, depth of burst, yield and maximum tensile stress. Typical stress fields are shown in Fig. 29 for various depths of burial. In the case of soil, one might expect parting along some natural layer where the tensile strength of the soil is less than the magnitude indicated.

For the purposes of the qualitative model we assume that separation of the earth caused by spalling takes place along some plane parallel to the earth's surface and, furthermore, that the spalled slab is thin compared to the depth of burst. At the instant of detonation a spherical shock wave propagates radially from the explosive source. For our present purposes, we assume that the magnitude of the peak particle velocity diminishes as the inverse first power of the distance from the source of the explosion. Hence we have

$$u = K/R \quad , \qquad (36)$$

where R is the radial distance from the source of the explosion;

u is the particle velocity at the distance R;

K is a proportionality constant.

The time, t_a, required for the shock wave to reach the surface at a distance, R, from the explosive source is given by

$$t_a = R/c \quad . \qquad (37)$$

where c is the propagation velocity.

Upon arrival of the direct disturbance at the surface, a rarefaction wave is

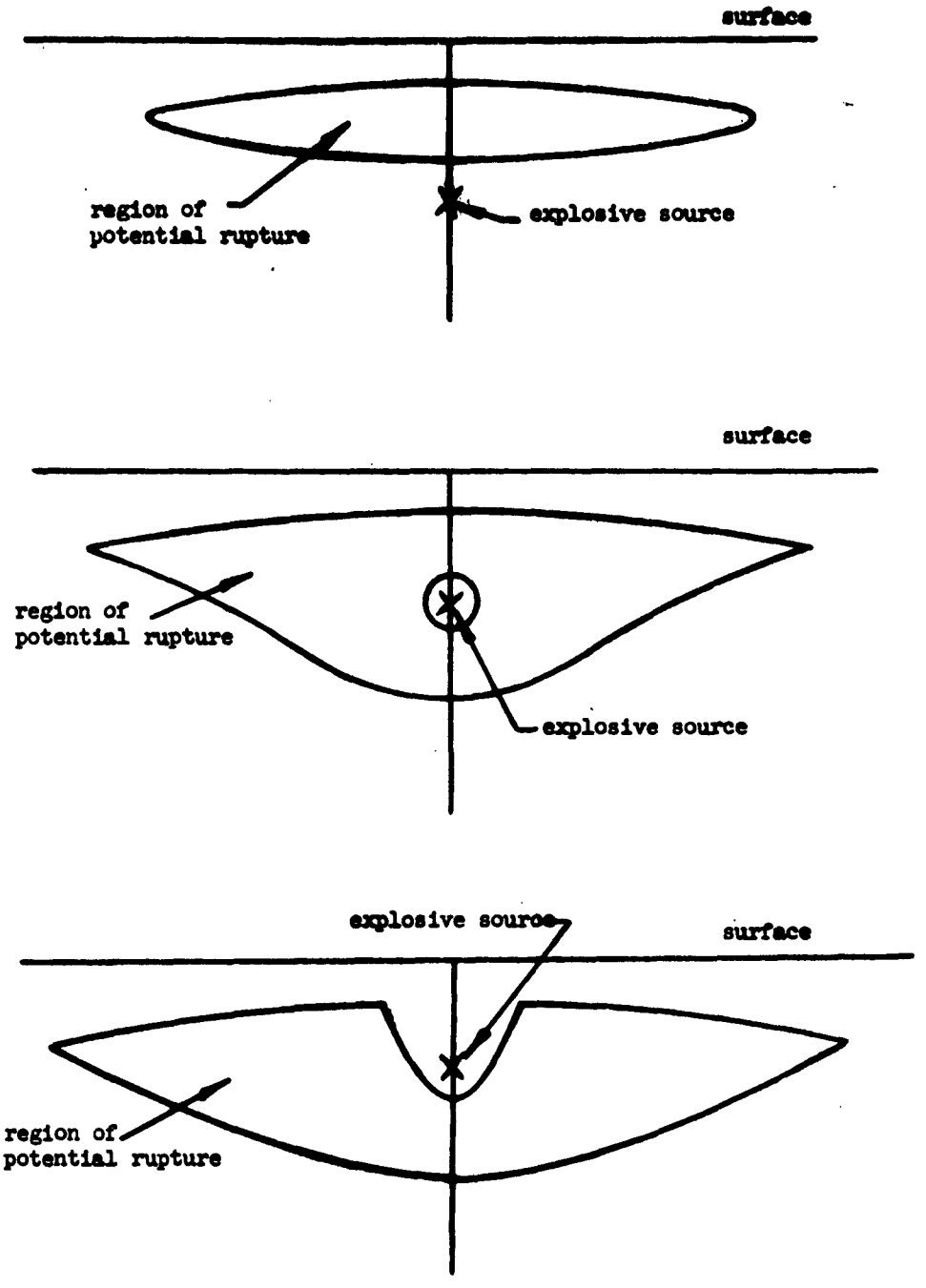

Fig. 29--Region in which spalling may begin for the same yield but three different depths of burst. The top figure is for a deep shot and the bottom figure is for a shallow shot. The existence of the gas globe has been neglected. The contour indicates the region under tensions in excess of some predetermined value.

generated and begins to propagate back into the soil. The rarefaction wave having a stress opposite in sign to the direct wave tends to relieve the stress in the soil. In this process, a portion of the potential energy is converted to kinetic energy which appears in the form of increased particle velocity. The velocity of the particles at the surface will be directed normal to the surface and have an amplitude approximately twice the amplitude of the direct wave just prior to impact with the surface.

With the occurrence of spalling we assume that the resulting slab is hurled upward at twice the particle velocity of the direct disturbance prior to impact; and that it is decelerated by the force of gravity alone. The flight time, t_s, of this spalled slug is then given by

$$t_s = 4u_v/g \quad , \qquad (38)$$

where u_v is the vertical component of particle velocity;

g is the acceleration of gravity.

The total time, T, to impact as measured from the time of detonation is

$$T = t_s + t_a \quad ,$$

or

$$T = R/c + 4u_v/g \quad . \qquad (39)$$

In terms of the particle velocity, u, we can write an expression for the vertical component, u_v

$$u_v = ud/R \quad , \qquad (40)$$

where d is the depth of burst.

Now, from Eq. (39) we can determine the horizontal distance at which first impact occurs.

$$h_f = \begin{cases} \left[\left[\left(\frac{8Kcd}{g}\right)^{2/3} - d^2\right]^{1/2}\right. & \text{for } d \leq \left[\frac{8Kcd}{g}\right]^{1/2} \\ 0 & \text{for } d > \left[\frac{8Kcd}{g}\right]^{1/2} \end{cases} , \qquad (41)$$

where h_f is the horizontal distance to the circle of first impact. This distance will define a circle of contact of the spalled slab with the underlying earth. (In the special case where first impact occurs below surface zero the circle of first impact will be a point.) In general there will be two circles of closure or impact: one traveling inward and one traveling outward from the circle of first impact. The configuration of the impacting slab shortly after the time of first impact is shown in Fig. 30 Plots of secondary wave arrival time and impact velocity versus radial distance are shown in Fig. 31. The velocity at which this closure or traveling circle of impact moves is given by the derivative of the horizontal distance, h, (where $R^2 = h^2 + d^2$) with respect to time, t, and can be obtained from Eq. (39). The horizontal velocity, V, of closure is found to be

$$\frac{dh}{dt} \equiv V = \frac{cR}{h}\left(1 - \frac{8Kcd}{gR^3}\right)^{-1} . \qquad (42)$$

For large horizontal distance, hence large slant range R, it is easy to see that this expression approaches the propagation velocity, c, of the medium.

Further evaluation of Eq. (42) shows that the inward traveling circle of impact travels first at velocities well above the seismic propagation velocity, c, in the medium but slows down quite rapidly and perhaps drops to velocities below

cross section view of spalled slab with contour exaggerated to show manner of impact.

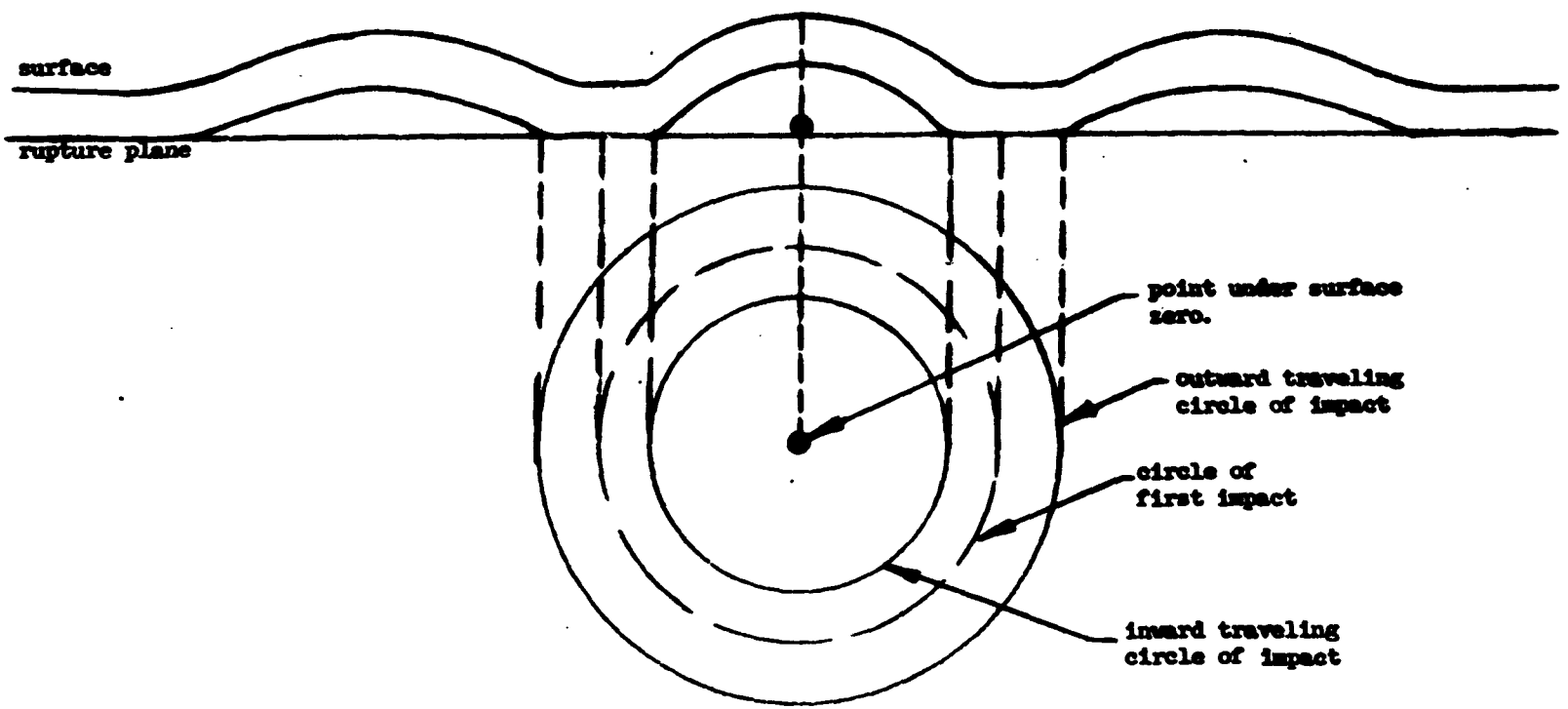

horizontal view of rupture plane.

Fig. 30--Spalled slab and its projection on the rupture plane shown just after initial impact.

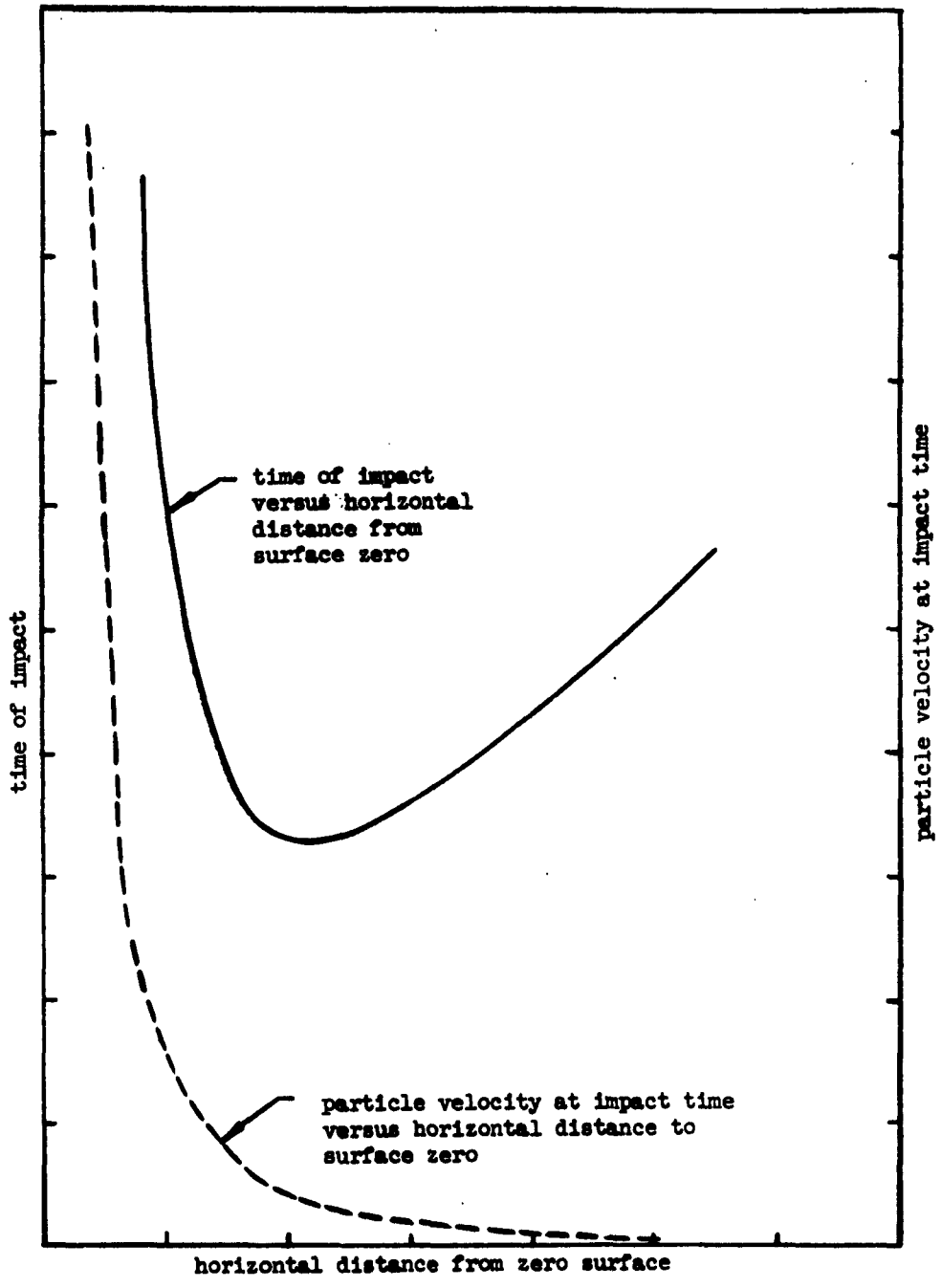

Fig. 31--Shows qualitative results of computations to determine time of impact and impact velocity.

the propagation velocity; finally, as the inward traveling circle of impact approaches the point directly under surface zero, the horizontal (inward) velocity of the circle of impact again increases to large values.

On the other hand, the circle of impact traveling outward from the circle of first impact will also start out at a very high velocity, again above propagation velocity of the medium, gradually slow down to the propagation velocity, c, with increasing distance from the explosion.

The impacting of the spall in this fashion produces a moving source of pressure, and we may now draw some qualitative conclusions as to the type of wave patterns which might be expected from such a moving source. Using a Huygens construction we may determine the position of the secondary waves soon after the time of first impact. Fig. 32a shows the shape of the wave front shortly after the time of first impact. Near the circle of first impact the closure or traveling impact point proceeds at supersonic velocity, and hence a bow shock will be produced. This bow shock will be at an angle, β, as shown in Fig. 32a, where β is given by

$$\beta = \text{arc sin } (1/M)$$

where M is the Mach number of the traveling circle of impact. Fig. 32b shows the secondary wave pattern well after the time when the inward traveling circle of impact has fallen below the propagation velocity of the medium. The dotted lines indicated in Fig. 32b denote gradual rise fronts, while the solid lines indicate quick rise or shock fronts. These gradual rise wave fronts occur because the inward traveling circle of impact has fallen below the medium's seismic propagation

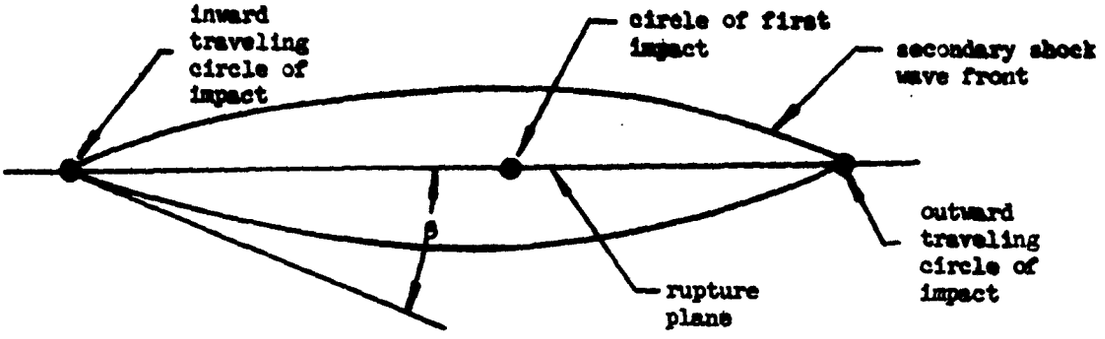

Fig. 32a--A secondary wave pattern soon after the time of first impact.

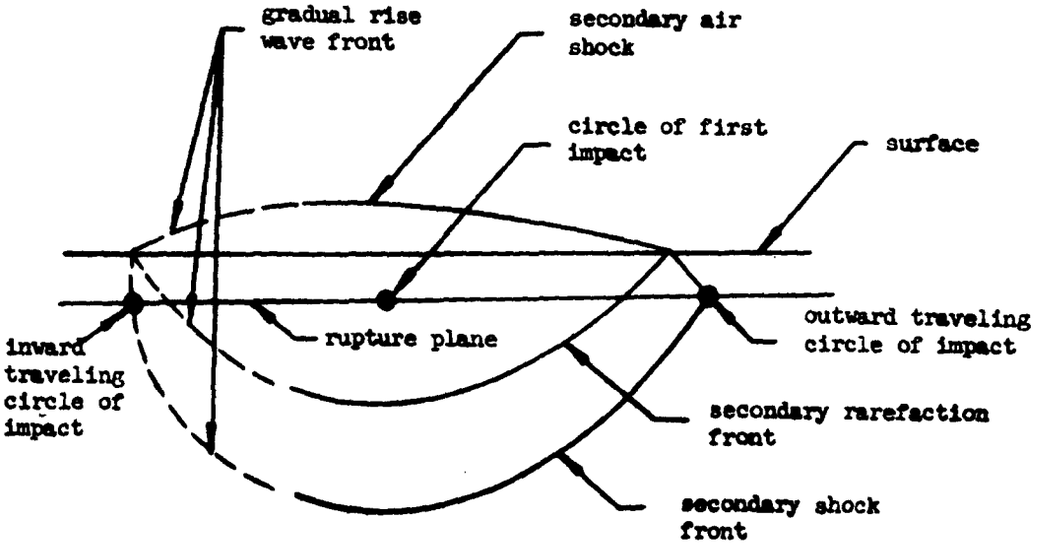

Fig. 32b--Secondary wave pattern at a time when the inward traveling circle of impact has fallen below sonic velocity.

velocity. In Fig. 32b we note that the outward traveling circle of first impact has associated with it a secondary shock front and that following closely behind is a rarefaction wave of very nearly equivalent magnitude. From constructions of this sort one can speculate on the secondary wave forms that would be recorded at any hypothetical gage in the field.

The foregoing analysis and discussion indicate that surface spallation phenomena will produce--as a consequence of the traveling point of impact or reloading--secondary stress disturbances which are quite distinct from the body waves emanating from an underground explosion. A more complete picture of these secondary waves now requires embellishment of the rudimentary theory presented here, together with numerical solution for configurations of interest. In any further analysis the theory should be extended to include such factors as: surface contour; geologic layering; variable propagation velocity, wave shape, and shearing forces.

VI. CONCLUSIONS

The object of this investigation has been to determine the wave shapes of the seismic disturbances that are generated by an underground nuclear explosion. The investigation took into account (1) the generation of the mechanical disturbances, (2) the propagation of these disturbances.

Two means of wave generation have been considered: (a) generation of waves from the expanding cavity (body waves); (b) generation of waves due to surface spall and subsequent impact. Additionally we have considered two types of wave propagation: (a) waves in crushable material and (b) waves in elastic material. These two means of propagation might be thought of as the two extreme ways in which waves can propagate in solid materials.

The elastic precursor, a wave shape detail of the direct or body wave disturbance, has been simply treated so as to show the the possible gains to be obtained from a more detailed study.

In the foregoing analysis, we have observed the following:

1. Details of the precursor may be significant in determining the behavior of the soil (details about the equation of state) in the region close in to a nuclear explosion. Also, this disturbance is the first received by a seismic station and, hence, will not be subject to interference from mechanical disturbances propagating along other paths from the same source. Therefore, more emphasis should be placed on instrumentation to determine the character of the leading edge, and on analysis to determine the expected shape of the leading edge.

2. Waves generated by surface spall and subsequent impact of the spall

may be used to gain information about the environment of the explosive source and, in particular, about the close-in geometry. Comparison of these secondary waves with the direct disturbance may yield important information about the mechanism of wave generation.

3. A simple crushable equation of state can be used in conjunction with equations of motion to determine the gross features of wave propagation in the crushable region near an explosive source. A more accurate analysis, if needed, should include the effect of variable density behind the wave front. Shearing forces should also be included in a more profound analysis, especially in respect to waves propagating through the region near the seismic transition zone. In the very close-in region, the analysis may need to include thermodynamic theory although, in the crushable region of our interest, it is believed that such an inclusion would cause only a perturbation to the results.

4. In the extension to the work reported herein, the authors are developing a general theoretical framework which covers the elastic and crushable wave analysis as special cases--and, importantly, should permit investigation between these two extremes.